Agricultural and Forest Meteorology 357 (2024) 110210

Contents lists available at ScienceDirect

Agricultural and Forest Meteorology

journal homepage: www.elsevier.com/locate/agrformet

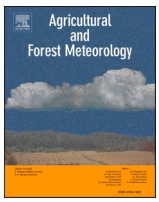

Modeling weather-driven long-distance dispersal of spruce budworm moths (*Choristoneura fumiferana*). Part 2: Flight model calibration using radar data

Matthew Garcia [a,*], Brian R. Sturtevant [b], Yan Boulanger [c], Jacques Régnière [c]

[a] Department of Forest and Wildlife Ecology, University of Wisconsin–Madison, Madison, WI 53706, USA
[b] USDA Forest Service, Northern Research Station, Rhinelander, WI 54501, USA
[c] Natural Resources Canada, Canadian Forest Service, Québec, QC G1V 4C7, Canada

ARTICLE INFO

Keywords:
Aerobiology
Dispersal
Individual-based modeling
Lepidoptera
Numerical modeling
Parameter calibration
Weather radar

ABSTRACT

In Part 1 of this series (Garcia et al., 2022), we introduced a novel individual-based model for the simulation of dispersal flight of adult spruce budworm (SBW: *Choristoneura fumiferana*) and demonstrated the results of that model under real weather conditions for two nights in July 2013 on which SBW mass dispersal events were observed by weather radar in southern Quebec, Canada. Here, following the selection of one uncertain parameter value using empirical measurements, we used those radar observations for the quantitative calibration of two uncertain flight model variables in our individual-based SBW–pyATM model, one that describes the conversion of moth wingbeat to flight speed, and a second that allows the moth to conserve energy during flight. For these experiments, we adapted a grid-based metric from meteorology that has previously been used to calibrate and validate precipitation forecasts by comparison with radar data. Through thousands of flight simulations for the night of 15–16 July 2013, examining each of these parameters separately and in conjunction, we arrived at optimal values that produce a spatiotemporal distribution of SBW moth dispersal that most closely matches the radar observations for that night. We then applied those calibrated parameter values to simulations of SBW dispersal on the night of 14–15 July 2013 and found a lesser but still reasonable resemblance to weather radar observations on that night as well. These two parameters have significant effects on the speed, altitude, and distance of dispersal, and are thus critical to the goal of estimating when and where SBW males and females land, with subsequent effects on reproductive behavior and the spatial redistribution of SBW populations over a dispersal season.

1. Introduction

It is becoming better recognized that insect dispersal events can be massive, wide-ranging, and transformative for spatiotemporal patterns of both insect populations and landscape ecology (Chapman et al., 2015; Hu et al., 2016; Landry and Parrott, 2016; Satterfield et al., 2020). Radar has been used to identify and track insect migrations and mass dispersal since at least the 1960s, with a focus primarily on agricultural pests in the Sahel region of Africa (Schaefer, 1969; Riley et al., 1979; Riley and Reynolds, 1983; Reynolds and Riley, 1988) and southern Australia (Drake et al., 1981; Drake and Farrow, 1983; Drake, 1984, 1985; Rennie, 2014). Similar studies have been undertaken in eastern Canada (Schafer, 1976, 1979; Dickison et al., 1983, 1986; Boulanger et al., 2017), the UK (Reynolds et al., 2005, 2008; Wood et al., 2006, 2009; C.R. 2010), China (Riley et al., 1994; Hu et al., 2019; Liu et al., 2021), and the United States (Beerwinkle et al., 1994; Westbrook et al., 2014; Westbrook and Eyster, 2017). Many such observational efforts have been reviewed by Chapman et al. (2011, 2015) and more recently by Bauer et al. (2019) and Becciu et al. (2019).

Efforts to understand the dispersal patterns of economically important agricultural and forest insect pests have prompted individual-based modeling of these events. Some such models have combined empirical studies of individual flight behavior in the target species with ready-made components for atmospheric dispersal. Using models based on HYSPLIT (Draxler and Hess, 1998; Stein et al., 2015), Westbrook et al. (2016, 2019) studied fall armyworm (*Spodoptera frugiperda*) dispersal, and Wang et al. (2019) and Koralewski et al. (2021) investigated sugarcane aphid (*Melanaphis sacchari*) dispersal, both by various pathways across the south-central US. However, each of these models treated the dispersing moths as inert, pollutant-like tracers in HYSPLIT that travel at

* Corresponding author.
E-mail address: megarcia@wisc.edu (M. Garcia).

https://doi.org/10.1016/j.agrformet.2024.110210
Received 2 November 2023; Received in revised form 23 August 2024; Accepted 28 August 2024

the speed of the wind, rather than as active agents with their own flight behavior.

Fundamental work in radar aeroecology has investigated the accuracy of Doppler radar techniques for wind speed retrieval using insects as signal targets (Rennie et al., 2010; Melnikov et al., 2014), and insects in radar observations can function as useful indicators of airflow patterns, especially in the convective boundary layer (Chandra et al., 2010) and around thunderstorms (Pedgley et al., 1982; Dickison et al., 1986; Browning et al., 2011). Studies have shown that tracking coherent masses, layers, and plumes of insects with Doppler (Rennie, 2014; Westbrook et al., 2014; Boulanger et al., 2017; Westbrook and Eyster, 2017) and polarimetric (Zrnic and Ryzhkov, 1998; Westbrook and Isard, 1999; Stepanian et al., 2016; Gauthreaux and Diehl, 2020) weather radars can provide detailed information useful to improving mechanistic descriptions of insect flight behavior. Advances in radar signal processing technology and spatiotemporal resolution have led to direct comparisons between radar observations and weather-based models of insect dispersal (Ainslie and Jackson, 2011), including a radar-based validation of an agricultural pest immigration forecast in Finland (Leskinen et al., 2011).

In Garcia et al. (2022), hereafter referred to as "Part 1″ in this series, we presented an individual-based model of dispersal flight by adult spruce budworm moths (SBW: *Choristoneura fumiferana* Clem.) (Lepidoptera: Tortricidae). An outbreak of SBW populations and expansion of defoliation areas in Quebec, Canada, and the surrounding provinces has been ongoing since ~2003 (Bouchard and Auger, 2014), significantly longer than the typical outbreak duration in that region with a range of 5 to 25 years, mean of 10.2 years, and standard deviation of 3.8 years (Boulanger and Arsenault, 2004; Boulanger et al., 2012). Outbreak longevity is driven in part by the availability of SBW host trees, primarily balsam fir (*Abies balsamea* L. Mill.) and white spruce (*Picea glauca* Moench Voss), their capacity to recover from larval herbivory, the survival of SBW from predators, parasites, and winter conditions, and the dispersal of the SBW as adult moths in above-canopy flight during summer.

It is this last mechanism on which we have focused in this series. This modeling effort can be traced directly from the seminal empirical work on SBW flight behavior in eastern Canada through radar observations by Schaefer (1976) and aerial sampling by Greenbank et al. (1980), which demonstrated that the SBW moths concentrated near the top of the nocturnal surface layer (100–200 m AGL) as it deepened through the nighttime flight period. Using those flight height observations, Sturtevant et al. (2013) combined individual-based SBW flight parameterizations with wind fields from the Weather Research and Forecasting (WRF) model (Skamarock and Klemp, 2008; Skamarock et al., 2008; Powers et al., 2017) to explain SBW dispersal and trap captures in northern Minnesota. However, subsequent radar observations of SBW dispersal in Quebec obtained by Boulanger et al. (2017) indicated flight heights up to ~1 km AGL, near the top of the atmospheric boundary layer and far above those reported in earlier observations by Greenbank et al. (1980). This finding led researchers to re-evaluate numerous assumptions regarding SBW flight physiology and behavior, resulting in the work by Régnière et al. (2019a, b) that synthesized decades of accumulated research into SBW flight mechanisms and mass dispersal behavior.

We combined the methodology for individual-based integration with WRF model fields developed by Sturtevant et al. (2013) with the physiological flight formulations presented by Régnière et al. (2019a, b) to develop the SBW flight model described in Part 1. In that work, our model was driven by wind and temperature fields from WRF model output specific to two nights during the period of peak SBW dispersal activity in July 2013 examined by Boulanger et al. (2017). In both Part 1 and this work, we compare our modeled SBW dispersal patterns with radar data over the St. Lawrence estuary from the Environment Canada weather surveillance (Doppler) radar located in Val d'Irène, Quebec (XAM; 48.4783°N, 67.5822°W, 722 m above mean sea level). While our comparisons between model results and radar observations in Part 1 were primarily qualitative, here we explore quantitative comparisons over those two nights, using one night's data for calibration and the other for validation.

The temperature and wind profiles in the boundary layer are critical inputs to this model: as the moth attains a flight altitude where its temperature-dependent wingbeat can offset its weight, it is the ambient wind at that level that determines the speed and direction of dispersal. Those can be far different from the winds at higher and lower levels in an atmospheric boundary layer that is shaped by the complex combination of topography, surface friction, synoptic wind patterns, and changing heat fluxes throughout the nocturnal transition period. Using scan-based profiles and upward-pointed radars, researchers in both Australia (Drake, 1984, 1985; Rennie, 2014) and the UK (Chapman et al., 2002; Reynolds et al., 2005, 2008; Wood et al., 2006, 2009) have explored the vertical distribution of insects in the boundary layer during dispersal events. Thermal stratification often leads to the organization of flying insects into coherent layers, generally with high concentrations of insects in warm air near the top of a nocturnal surface or boundary layer inversion (Greenbank et al., 1980; Drake, 1984; Wood et al., 2006, 2010; Reynolds et al., 2009). Our model results presented in Part 1 were consistent with these patterns, with high concentrations of moths at select altitudes during each night of dispersal simulations.

There are three aspects of SBW flight behavior that we relate to the flight patterns observed by radar: moth concentration, location, and direction of motion. In Part 1 we established the fundamental characterizations of SBW moth flight that are key to the relationship between our model results and radar observations: the SBW moth in dispersal flight is an active (but not necessarily strong) flier that moves in the same direction as the wind, controlling its altitude according to temperature-driven wingbeat, and by that wingbeat also moving slower than the wind itself.

Between the temperature-dependent mechanics of SBW flight (Régnière et al., 2019a) and observations on the crepuscular activity and evening initiation of SBW mass dispersal flights (Régnière et al., 2019b), there remain uncertainties in several aspects of SBW flight mechanics and the wind-driven aerial dispersal process. Here, we examine three relatively uncertain model parameters related to SBW liftoff timing and flight behavior that have not yet been either observed directly in the field or deduced from laboratory measurements. Where Part 1 showed qualitative comparisons between simulated SBW flight trajectories and weather radar observations, here we perform thousands of flight simulations and quantitative model/radar comparisons on the same two nights of July 2013. Drawing from precipitation forecast validation metrics in meteorology, we advance the discipline of radar aerobiology for empirically based modeling of insect dispersal through quantitative verification metrics. We explore the modeled response in dispersal behavior across ranges of likely values for two of these three important flight parameters, using the radar data to guide our selection of the most likely parameter values for future use.

2. Study area, model inputs, and radar data

Aerial surveys of forest defoliation (MacLean and MacKinnon, 1996; Taylor and MacLean, 2008) indicated that, by 2013, approximately 3.2 M ha of eastern Canadian spruce–fir forest in the St. Jean Lake, North Shore, and Lower St. Lawrence regions of Quebec were affected by an outbreak of SBW that had been ongoing since ~2003 (Bouchard and Auger, 2014) (Fig. 1a). In Part 1 of this series, we focused on simulating SBW dispersal flights from known areas of forest host defoliation in southern Quebec starting around sunset on the evenings of 14 and 15 July 2013. To support our individual-based model of moth flight, we used wind and temperature output grids at high spatiotemporal resolution ($\Delta x = 3$ km and $\Delta t = 1$ h) for those two nights from the WRF model with large-scale forcing provided by the NOAA–NCEP North American Regional Reanalysis (NARR; Mesinger et al., 2006; Luo et al.,

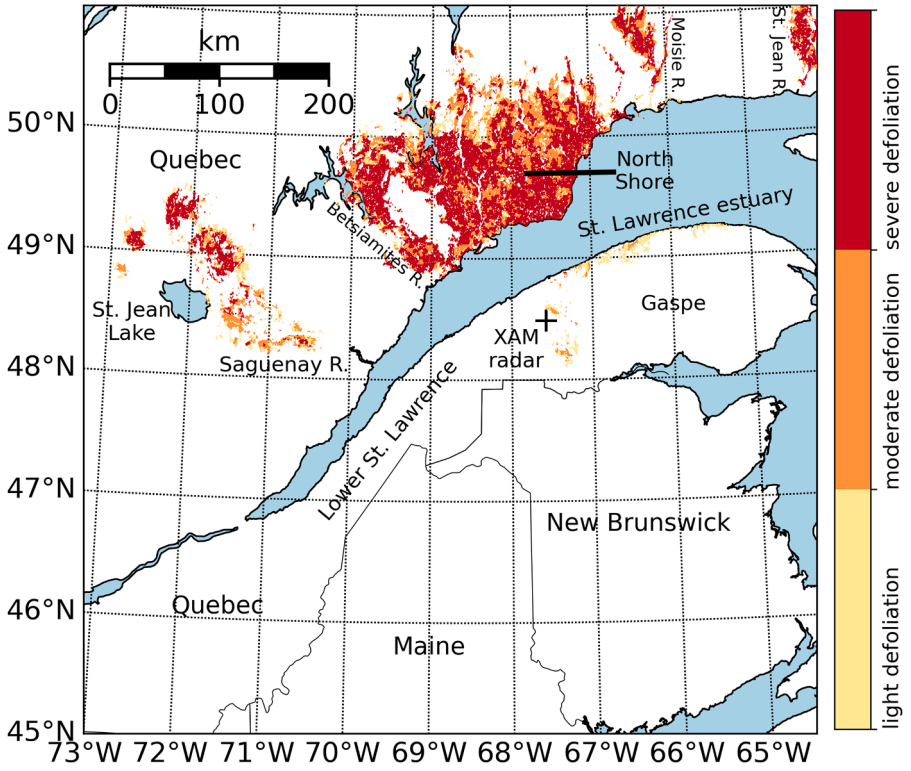

Fig. 1a. Defoliation severity in SBW host forests in eastern Canada and the northeastern United States, based on aerial surveys in the summer of 2013.

2007). Moth liftoff locations for each night were obtained using BioSIM, a system developed by the Canadian Forest Service to collect available weather station data and generate daily temperature maps (Régnière and Bolstad, 1994; Régnière, 1996; Régnière and Saint-Amant, 2007) as input to individual-based insect seasonal biology models (Régnière et al. 1995; Régnière, 1996; Régnière et al., 2014), including that for SBW (Régnière et al., 2012). Our uses of both WRF and BioSIM were described in detail in Part 1.

Our modeling results showed that large numbers of SBW moths dispersed across the St. Lawrence estuary primarily eastward from the

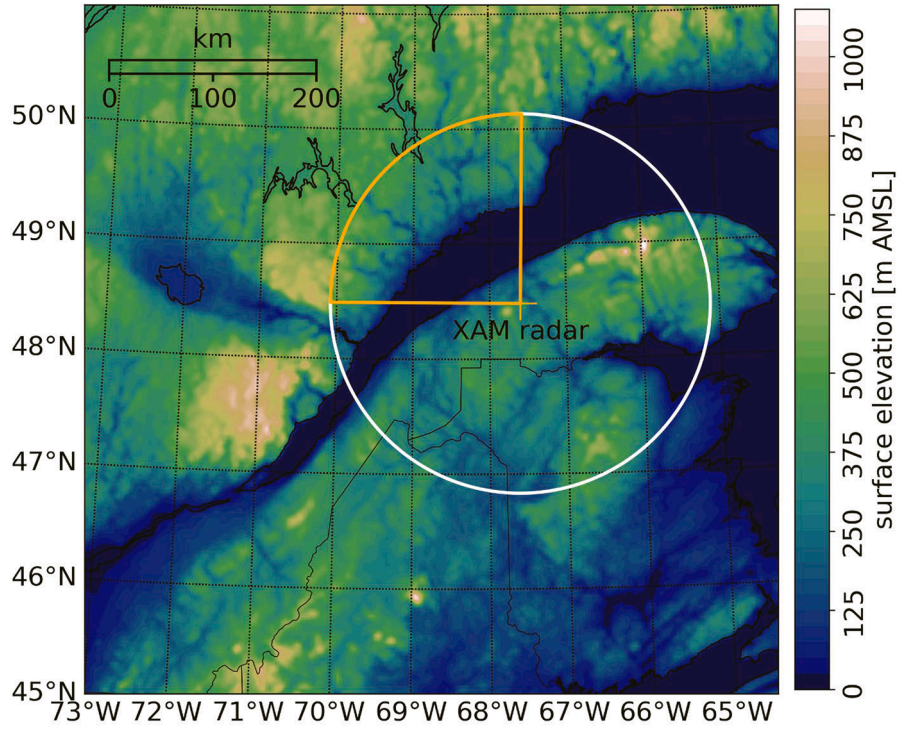

Fig. 1b. Approximate coverage area of the Val d'Iréne (XAM) weather surveillance radar (white circle) in southern Quebec, Canada, with the northwest quadrant sub-area used for calculations of SBW–pyATM simulation accuracy outlined in orange.

St. Jean Lake region on the night of 14–15 July 2013 (Part 1, Fig. 4), and primarily southward from the St. Jean Lake and North Shore regions on the night of 15–16 July 2013 (Part 1, Fig. 7). Both SBW dispersal flight events were observed by the Val d'Irène weather surveillance (Doppler) radar (XAM; 48.4783°N, 67.5822°W, 722 m AMSL; location and approximate coverage area marked in Fig. 1b). The XAM weather radar is special not only for its location within the southern Quebec outbreak region but also because its scan strategy includes angles with a downward tilt, such that the radar can observe locations close to the surface over and across the St. Lawrence estuary into the North Shore (Gagnon et al., 2011; Boulanger et al., 2017). Our results in Part 1 showed that the SBW flights occurred in layers well below elevations that a typical radar surveillance strategy (angles above 0° beam elevation) would scan. As a result, however, in most of the XAM coverage area there are significant arcs that topography blocks from view at those low radar elevation angles. To minimize interference from surface clutter and false targets in our comparisons between simulated flights and radar observations, we use only the northwestern quarter of the XAM radar coverage area, over the St. Lawrence estuary and a small part of the North Shore region between Tadoussac in the east and Sept-Îles in the west, for these quantitative analyses.

3. Methods

Following the model description presented in Part 1, here we examine the variability in model results due to uncertainty in the values of three computational flight parameters. We then compare simulated spatiotemporal patterns of flying SBW moths during the night of 15–16 July 2013 with empirical expectations and with the available XAM radar observations, using a metric method adapted from meteorological forecasting, to select the most likely values for these model parameters. We then evaluate the accuracy of our calibrated flight simulations using XAM observations on the night of 14–15 July 2013 using the same metric. Each step of this process is described below.

3.1. Model overview

The formulation of our Python-based Atmospheric Transport Model for Spruce Budworm (SBW–pyATM) was described in detail using the "Overview, Design, and Details" protocol for individual-based models (Grimm et al., 2006, 2010) in Part 1 of this series, and is summarized here. The locations and availability of SBW adult moths in the surveyed outbreak area (Fig. 1a), following emergence from the pupa and mating, are provided by the BioSIM modeling framework. Moth liftoff, flight, and landing are driven by weather conditions using WRF simulation output to account for radiative cooling and nocturnal transitions in boundary layer temperature and wind profiles throughout the study area, including terrain effects on low-altitude winds. The SBW–pyATM framework accounts for SBW sexual dimorphism (see Régnière et al., 2019a) and its effects on the physical flight capability of dispersing moths. The model allows for ensemble simulations, using random selections of available moths within the study area, to represent large dispersal events. Each simulated SBW moth is an individual with unique information regarding its traits such as sex, morphology (mass and wing size, and eggs carried by females), location (including altitude), environment (temperature, three-dimensional wind speed, and precipitation), and flight activity (flight phase, wingbeat, wind-relative flight speed) throughout the simulation. All moths in the simulation are subjected to a common set of behavioral rules regarding the effects of their environment in the forest canopy, at liftoff, and during dispersal flight and landing. Model tracking of individual female SBW fecundity can provide location-based estimates of egg quantities likely deposited prior to liftoff and after landing, as illustrated in Part 1.

During model execution, each dispersing moth can go through three flight phases according to the imposed computational and environmental conditions. In the liftoff phase, the decision to lift off from the forest canopy is determined by three factors: a "readiness" function calculated from time of day (Régnière et al., 2019b), warm enough temperatures to support a wingbeat necessary for flight (Régnière et al., 2019a), and a minimum wind speed required for liftoff $V_{h,\min}$ that is based on empirical observations by Greenbank et al. (1980). This last condition for liftoff, defined formally in Part 1, Eq. (1), remains the most uncertain and is explored in more detail here. During the flight phase, moth activity is determined primarily by the temperature–wingbeat relation (Régnière et al., 2019a). Within those dynamics, however, there are two more aspects of the physical description that remain uncertain: first, the conversion of wingbeat to forward motion, coefficient ε defined in Part 1, Eq. (6), which depends in part on individual moth morphology (wing size and weight), and second, the possibility that the moth may conserve energy by reducing its wingbeat frequency through the parameter Δ_ν, defined by Régnière et al. (2019a), Eq. (11), but which was not used in our Part 1 simulations under the assumption that $\Delta_\nu = 1.0$. Thus, three parameters from the morphologically based flight functions in our model were not directly measured or estimated from empirical observations of SBW flight behavior and were targeted for calibration here.

3.2. Uncertain model parameters

3.2.1. Minimum wind speed for liftoff, $V_{h,min}$

Greenbank et al. (1980) observed that SBW moths do not fly under "calm" conditions. We included this restriction in Part 1 as $V_h < V_{h,\min}$, where V_h is the horizontal wind speed near the surface (provided by WRF) and $V_{h,\min}$ is a specified threshold wind speed below which a moth will not lift off. Preliminary modeling tests for Part 1 suggested that the combination of diurnal readiness for flight (Régnière et al., 2019b) and the imposition of a minimum wind speed for liftoff could either reinforce or interfere with each other. As winds during summer can often increase in the afternoon and then slow after sunset, the likelihood that a moth will experience adequate winds for flight is constantly changing; the moth may attempt to lift off in calm conditions but, without a supporting wind, it must fly under its own power and is not likely to attain a large dispersal distance. At the same time, cooling air throughout the evening reduces the moth's capability for liftoff and dispersal flight. The objective for the (simulated) moth is then to lift off from the forest canopy in a narrow temporal window, the evening crepuscular period, when both wind and temperature support sustained flight activity and thus dispersal over some distance. Here we evaluate the sensitivity in the timing of simulated moth liftoff to wind speed V_h near the surface by varying the value of $V_{h,\min}$ over a range from 0.0 m s^{-1} (calm) to 5.0 m s^{-1} (moderate winds), at intervals of 0.25 m s^{-1}. Although winds less than that speed may still occur, a moth is allowed to lift off only in winds exceeding $V_{h,\min}$ during the period of diurnal readiness; our goal here is to determine whether any particular value of $V_{h,\min}$ interferes with moth liftoff and causes the simulated pattern to deviate from the expected temporal distribution in the crepuscular period described by Régnière et al. (2019b).

We note that some moths in our simulations simply did not fly at all. Nearly 80 % of the simulated moths on the evening of 14 July 2013 participated in the dispersal event, of which 61 % were males and 39 % were females. For simulations on the evening of 15 July 2013, 67 % of the simulated moths dispersed, with the same distribution between males and females even though this was not specified *a priori*. In our experiments, each simulation started with 1000 moths distributed randomly in areas of known SBW defoliation across the study area (Fig. 1a). The crepuscular readiness for flight (Régnière et al., 2019b) increases and then decreases over the evening, and wind speeds are somewhat random but generally diminish through the evening. In each simulation, there were moths that experienced adequate winds and temperatures but were just not ready to fly, were ready to fly but never had adequate wind speeds to allow their liftoff, or were ready to fly but the temperature had fallen too low to support their liftoff (Régnière

et al., 2019a). With these constraints, some moths simply do not undertake a dispersal flight in our simulations, and this fraction was highly consistent across ensemble simulations for each night.

Finally, we note for clarity that our model does not include a $V_{h,\max}$ condition to indicate a wind speed threshold above which the simulated moths would not lift off. We have found no observations to suggest SBW moths do not attempt above-canopy flight in strong winds. Indeed, numerous insect taxa have been observed to take advantage of strong winds in near-surface density currents and gust fronts for regional dispersal (McManus, 1988; Westbrook and Isard, 1999; Geerts and Miao, 2005; Geerts et al., 2006; Lothon et al., 2011), including SBW from radar observations of frontal passages (Dickison et al., 1983) and storm events (Dickison et al., 1986) over the same region we examine in this work.

3.2.2. *Conversion of wingbeat to flight speed, ε*

In Part 1, we formulated the SBW flight speed as suggested by Régnière et al. (2019a) and proposed the likely importance of a morphological flight strength $s = A / M$, the inverse of wing load as defined by Rhainds (2020), with the area of a single forewing A [cm^2] and moth dry mass M [g]. The wingbeat coefficient ε then combines with flight strength s to influence the conversion of wingbeat to moth (wind-relative) vertical propulsion:

$$v_z = \varepsilon\ s\ [\nu(T) - \nu_s] \tag{1}$$

where ε has units of [m s^{-1} g cm^{-2} Hz^{-1}] and v_z is in [m s^{-1}]. The wingbeat frequency ν_s [Hz] corresponds to settled (level) flight that depends strictly on moth morphology:

$$\nu_s = K\ \frac{\sqrt{M}}{A} \tag{2}$$

as in Régnière et al. (2019a), with $K = 167.5$ Hz $cm^2\ g^{-1/2}$ as determined there. The actual wingbeat frequency $\nu(T)$ [Hz] is a sigmoidal function that depends on temperature:

$$\nu(T) = \frac{\nu_{max}}{1 + e^{-b(T-a)}} \tag{3}$$

as in Régnière et al. (2019a), where T [°C] is ambient temperature, ν_{max} [Hz] is the maximum wingbeat frequency for SBW moths, a [°C] is the midpoint temperature of the wingbeat response, and b [$°C^{-1}$] is the spread of that response with respect to temperature. Régnière et al. (2019a) determined that $\nu_{max} = 72.5$ Hz, $a = 23.0$ °C, and $b = 0.115$ $°C^{-1}$ for SBW moths, which we have used here without the associated uncertainties. Overall, Eq. (1) represents the work done by the moth to offset its own weight and remain aloft while it is carried downstream by the horizontal wind. Given that the boundary layer wind speed and direction can change significantly with height, the key here is to ensure that the moth reaches a flight height that is consistent with its physiological response to the ambient temperature.

While developing the SBW flight model using the fundamental relations provided by Régnière et al. (2019a), we started our experiments with the assumption that the moths moved faster than the horizontal wind, specifically using the estimated flight speed from Greenbank et al. (1980) that was also employed by Sturtevant et al. (2013). In those initial results, we found that the simulated moths moved across the St. Lawrence River far faster than the radar observations indicated. We then parameterized the moth flight speed in a manner like Eq. (1) as a function of the flight strength and wingbeat, which is itself a direct response to the environmental temperature (Régnière et al., 2019a), but without the settled wingbeat factor. However, the moths in those results were still too fast compared to the radar observations. When we tried $v_h = 0.0$, analogous to a moth hovering while the wind carried it along (as for the inert or passive tracers in HYSPLIT-based models), the speed at which the moths transited the St. Lawrence River was still somewhat faster than the radar observations indicated, but the results were closer than positive forward flight speeds had provided. We then reversed the sign of the parameterized horizontal flight speed:

$$v_h = -\ \varepsilon\ s\ \nu(T) \tag{4}$$

where all terms on the right side have the same values and units as in Eq. (1) and v_h is in [m s^{-1}]. With this formulation, modeled moth transit speeds over the St. Lawrence River converged with those suggested by the radar observations, and the problem was then reduced to explaining this seemingly counterintuitive result and calibrating the ε parameter against those observations.

In our conceptual picture of the SBW moth in dispersal flight, the moth is not oriented upwind, as the negative sign in Eq. (4) might suggest, but rather faces downwind, in keeping with prior observations by Schaefer (1976, 1979) and Greenbank et al. (1980). We draw on observations of hawkmoth (*Manduca sexta*) flight as described by Willmott and Ellington (1997a, b). Hovering—of which only some insect species are capable—requires a more upright body orientation and horizontal wingbeat path (tracing the tip of the wing through its downstroke/upstroke cycle) than forward flight, and this rotation is further enhanced by the action of the wind on the SBW's unpowered rear (stabilizer) wings. Fig. 2a shows the free-body forces during hovering flight (see Willmott and Ellington, 1997a, Fig. 2), where the vertical components of lift (L_z) and thrust (T_z) offset that of the moth's weight (W_z), and the horizontal components of lift (L_x) and thrust (T_x) offset each other. Small-scale temporal variability due to the wingbeat motion exists (see Willmott and Ellington, 1997b, Fig. 3), but this is generally the dynamic force balance at work. This state can only exist if there is wingbeat motion that generates lift (by forcing air over the wing) and upward/forward thrust (because the wing is flexible). Adding wind in the $+x$ direction (Fig. 2b) induces form drag (D_x) on the moth, accelerating it downstream. The wind against the rear stabilizer wings exerts a torque that turns the moth slightly more vertical, making the lift force more horizontal (into the wind) and the thrust more vertical (less downwind). With this altered geometry of forces, the moth never quite attains the same ground-relative speed as the wind because *it actively opposes the flow* while being dragged along downstream.

Above the forest canopy, given sufficient winds for dispersal, we suggest that the individual moth is oriented as in Fig. 2b, with the wind at its back. The moth's only action, despite the additional energy required to "hover" (Willmott and Ellington, 1997b) over a long flight, is to oppose gravity and keep itself aloft; its self-powered flight is vertically upward while the ambient wind does the rest of the work moving it downstream. Adding the wind speed to the (negative) moth speed still leads to downwind displacement and overall geographic dispersal, especially in strong winds above the forest canopy. In cases where a moth already in flight encounters very weak winds, our model allows the moth to continue flying under its own power in the downwind direction with a lower body angle (see Willmott and Ellington, 1997a, Fig. 7, and 1997b, Fig. 3), and if absolutely calm winds are encountered then the moth continues in the same direction it last had until it reaches another location with non-zero wind. We emphasize that flight above the forest canopy is not goal-oriented: during wind-driven dispersal flight, the moth does not necessarily "aim" where it wants to go. We propose that directed (self-powered horizontal) flight occurs only in below-canopy and low-wind situations, such as when the male moth is following a pheromone trail to seek a mate or when a female is seeking a suitable host tree for egg deposition. Our model does not treat those phases of SBW flight.

For simplicity, we have assumed that ε is a constant and uniform characteristic of SBW morphology. Given a realistic crepuscular pattern of SBW liftoff on a night of known dispersal flight activity, we determined the appropriate value for ε by comparing the simulated SBW spatial concentration and motion throughout the evening with XAM radar reflectivity as an indicator of moth number concentration. The procedure for these comparisons is described below.

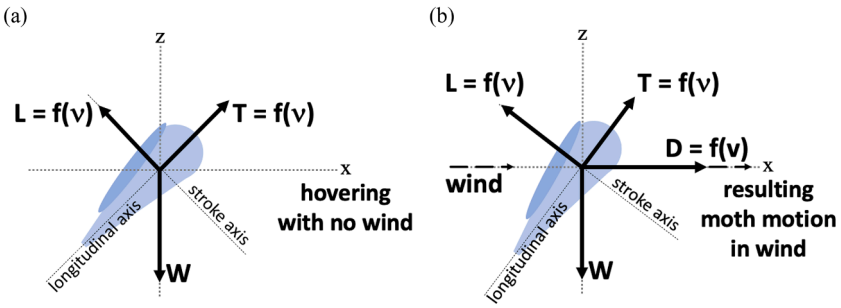

Fig. 2. Moth diagrams illustrating body orientation and related forces (a) while hovering, and (b) in a wind field. These states correspond to Willmott and Ellington's (1997a) Fig. 2 and Fig. 7 (upper left panel). Force vectors and angles are not to scale.

3.2.3. *Conserving energy in flight, Δ_ν*

The proportion Δ_ν (with absolute limits $0 \leq \Delta_\nu \leq 1$) was introduced by Régnière et al. (2019a) as an "energy conservation factor" to allow a flying moth to maintain sustained flight while reducing its wingbeat frequency from the strict temperature response in Eq. (3) by the factor Δ_ν. The reduced wingbeat frequency does not apply during liftoff when the temperature must still be high enough to produce a wingbeat frequency that can support the moth's weight, that is, $\nu(T) > \nu_s$. This reduction factor takes effect only once the moth reaches its first flight apex, where $v_z = 0$ and

$$\nu(T) = K \frac{\sqrt{M}}{A} \tag{5}$$

and is used to modify the value of $\nu(T)$ in Eqs. (1) and (4) above:

$$v_z = \varepsilon\, s\, [\nu(T)\, \Delta_\nu - \nu_s] \tag{6}$$

$$v_h = -\,\varepsilon\, s\, \nu(T)\, \Delta_\nu \tag{7}$$

Once the Δ_ν factor is enabled, it remains in effect for the remainder of the moth's flight. As with ε, we assume that Δ_ν is constant and homogeneous throughout the simulated moth population.

Régnière et al. (2019a) explored the general effects of Δ_ν on moth flight altitude with an idealized, one-dimensional model and showed that lower values of Δ_ν were associated with lower altitudes of the mean and peak SBW concentrations within the flight vertical profile. In a well-mixed boundary layer, such as during the daytime, or in a weak inversion layer near the surface at night, this means the moth would settle into cruising flight at a slightly greater temperature (lower altitude) without increasing its wingbeat to strict consistency with Eq. (2). In a strong inversion layer, such as the later nighttime boundary layer where the temperature increases with altitude up to the top of the surface layer and then cools beyond there (see Stull, 1988, Figs. 1.5, 1.7, and 1.12), this wingbeat reduction factor could have strongly opposing results: if the moth is already above the surface inversion layer when the factor is enabled, it may settle into cruising flight, but if its flight peaks within a cold layer, it would then descend and be driven to land almost immediately. Again, the timing of liftoff is crucial to the moth's successful dispersal from its location of origin.

In addition to the thermal structure of the boundary layer, this effect on flight altitude can have a strong influence on overall dispersal distance and direction given boundary layer winds that may vary considerably with height. Depending on the vertical profile of the horizontal wind speed, a reduced altitude could place the moths in faster or slower winds (and on a different heading) than at the higher level. In a stably stratified boundary layer, it is common to see smaller wind speeds near the surface and greater wind speeds near the top of the boundary layer where they are most affected by synoptic weather gradients. In such a case, moths dropping below their $\Delta_\nu = 1.0$ (temperature-dictated) flight altitude may move slower horizontally and thus disperse over shorter distances. Here we examine the changes in spatial patterns of SBW flights and ultimate landing locations in response to those effects.

Finally, we recognize that the wingbeat coefficient ε and the energy conservation factor Δ_ν could interact in their effects on ground-relative flight speed, flight direction, and total dispersal distance. Depending on the situation, these two factors could either offset or reinforce each other to produce the simulated outcomes. We thus extend our analysis beyond the determination of individual parameter values to include potential interactions when varying ε and Δ_ν together.

3.3. *Dispersal model computation*

All simulated moths are subjected to a common set of behavioral rules regarding response to their environment in the forest canopy, at liftoff, during dispersal flight, and when landing. All aspects of each moth's activity are recorded on a minute-by-minute basis over the course of a simulated night. A complete picture of each moth's physical state and environment can be reconstructed from its simulation time-series record to illustrate the influence of the changing structure of the WRF-described atmospheric boundary layer through the evening and overnight in response to surface heating, radiative cooling, and variations in topography. The SBW moths do not interact with each other during the flight simulation, and the only variations within an experiment (a unique set of parameter values with 500 replicate simulations) occur in the initial locations, physical characteristics, and liftoff times of the moths themselves. There is no variation in weather conditions across the simulation experiments for the night of 15–16 July 2013. Our distributed Monte Carlo approach to each experiment generates an ensemble of replicate results that we can then combine to illustrate a dispersal flight event much larger than computational resources would allow in a single simulation. We also use end-of-simulation post-processing routines to summarize the statistical outcomes of numerous simulations across the explored parameter spaces. We have made extensive use of computational resources at the University of Wisconsin–Madison Center for High Throughput Computing, 2006 and the Open Science Consortium (OSG, 2006; Pordes et al., 2007; Sfiligoi et al., 2009) for this work.

3.4. *Comparisons with radar data*

To facilitate comparisons across experimental configurations in our approach to model-based radar aerobiology, we adapted a validation method from radar meteorology. Radar observations are often used to evaluate, correct, and now initialize weather model forecasts, such as high-resolution simulations of precipitation and storm events (Bachmann et al., 2019). The Fractions Skill Score (*FSS*; Roberts and Lean, 2008) was devised to assess model simulations of precipitation intensity and location against weather radar reflectivity observations. Here, we use a simplified variation on the *FSS* metric to compare simulated concentrations of moths in flight with weather radar reflectivity observations. To our knowledge, this is the first such quantitative application of weather radar data to an insect dispersal model, and especially to the calibration of flight parameters in that model.

For this calculation, we recorded the locations of all flying moths at every minute of a simulation, mapped moth concentrations to match the XAM radar grid, and then combined these maps across all replicates of the same simulation conditions to assess moth concentrations and spatial variability. Collecting 500 replicate simulations for each experiment described here, the largest number concentration in a grid cell at any time was ~100 moths. We then compared the simulated and radar-observed concentrations at the same time using our modified version of the *FSS*. Unlike in comparisons between radar and simulated precipitation, we do not apply any bias correction or other adjustments before comparison. Our goal here is only to evaluate the two-dimensional spatial correspondence between radar observations and simulated moth densities at their own scales (we have excluded vertical profiles in this work). Our calculation differs from that for the *FSS* as described by Roberts and Lean (2008) in that we do not consider selected neighborhoods at multiple spatial scales, but instead look at a single "neighborhood" covering the northwestern quadrant of XAM radar coverage, simplifying our evaluation significantly. We also do not include a "reference" (*i.e.*, random) forecast or simulation, as was factored into the original *FSS* formulation.

As an example of our simplified calculation, consider an idealized radar observation (in units of dBz) and a hypothetical simulated moth density map (in units of moths per grid cell) on grids of 100×100 pixels (cells) at the same spatial scale, as shown in Fig. 3. For the calculations that follow, we divide the measured range of values on each map into five quantiles q of equal width (for the purposes of this illustration; we use ten equal-width quantiles in the results below), where $q = 1$ includes the smallest values and $q = 5$ includes the largest values. It does not matter that the quantiles may not match in unit or size across the two maps, only that the maps are divided into the same number of quantiles. Table 2 lists the quantile values and related area calculations for the example maps in Fig. 3. As for the *FSS* calculation, our modified *FSS* (*MFSS*) calculation uses the area covered by all quantiles at and above the given quantile, not just the area covered by a single quantile, and is illustrated in Fig. 4 and Table 3. We then sum the areas (pixels) of intersections I and unions U between simulated and radar images across all quantiles before dividing to obtain the overall *MFSS* for these two maps:

$$MFSS = \sum_{q=1}^{n} I_q \Big/ \sum_{q=1}^{n} U_q \tag{8}$$

Multiple counting of the areas of higher quantiles is mitigated by doing the same for both maps, not just one of them, reducing any non-equivalence penalty so that the overall score closely represents the overlap in overall footprint areas. In a perfect simulation, the intersection and the union of the two maps at the same quantile q would match, giving $I_q = U_q$ and $MFSS_q = 1.0$, with an overall $MFSS = 1.0$, just as proposed for the *FSS* calculation (Roberts and Lean, 2008). When the areas represented by the same quantile in each map differ in location, the intersection is smaller than the union, and the value of $MFSS_q$ diminishes from unity until $MFSS_q = 0.0$ when no overlap occurs (*e.g.*, quantiles 4 and 5). The overall *MFSS* also diminishes accordingly.

Using the XAM radar observations and our simulations of moth dispersal flights for the night of 15–16 July 2013 to perform these calculations, we then plotted the quadrant-scale *MFSS* values at 10 min intervals over the duration of the simulation, from 2100 UTC (1700 LDT, well before sunset) on 15 July through approximately 0910 UTC (0510 LDT, just after sunrise) the next morning, and use the mean of the *MFSS* time series to represent the overall simulation accuracy in comparison with the XAM radar observations. Our best calibration outcome had an increasing *MFSS* through the night as more moths joined the dispersal flight pattern, so we used both the maximum overnight value $MFSS_{max}$ and the average overnight value $MFSS_{mean}$ to select the best values of the tested flight parameters.

4. Results

4.1. Minimum wind speed for liftoff, $V_{h,min}$

The minimum horizontal wind speed for liftoff $V_{h.\min}$ affects the proportion of moths that can undertake flight at a given moment through the evening (Fig. 5a). The proportion of moths lifting off drops considerably with $V_{h.\min} > 2.0$ m s^{-1}, to the extent that almost no moths attempt to fly at $V_{h.\min} = 5.0$ m s^{-1}. For values below $V_{h.\min} = 2.0$ m s^{-1}, however, there is no effect at all of $V_{h.\min}$ on liftoff rates. Considering again that SBW moths have been observed to fly close to the ground but rarely in dispersal flight in calm conditions (Greenbank et al., 1980), which we interpret as $V_{h.\min} < 1.0$ m s^{-1}, we have selected an intermediate value of $V_{h.\min} = 1.5$ m s^{-1} for the remainder of our numerical experiments. This does not mean that winds at lesser speeds do not occur near the surface, only that the moths are not allowed to lift off at those wind speeds. With that value, we found that 65–85 % of the initialized moths participated in dispersal flights on the two simulated nights, depending on individual diurnal readiness (Régnière et al., 2019b) and immediate weather conditions. This value of $V_{h.\min}$ is further supported when we examine the effect of this parameter on flight timing (Fig. 5b): low values of $V_{h.\min}$ produce little difference in the median time of liftoff, approximately 30 min before both sunset and the theoretical median time for liftoff as determined by circadian crepuscular activity (Régnière

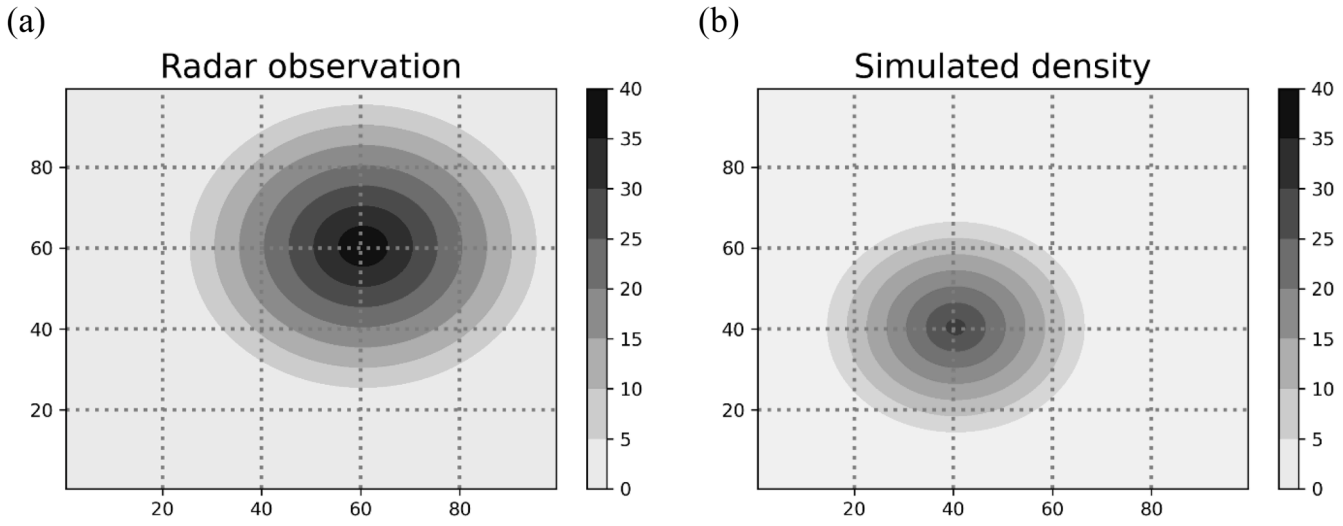

Fig. 3. Example input fields for calculating the modified Fractions Skill Score (*MFSS*).

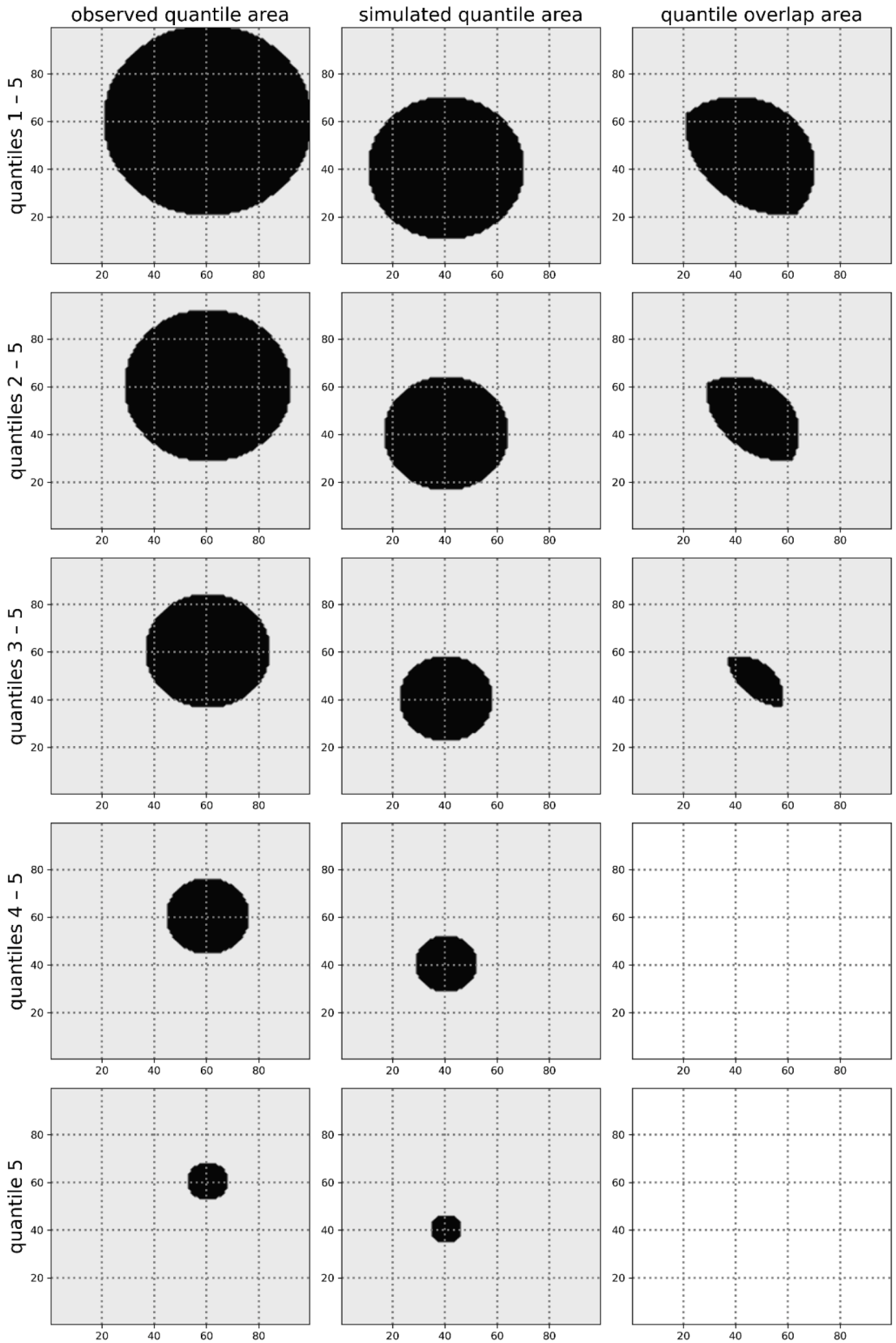

Fig. 4. Illustration of the example modified Fractions Skill Score (*MFSS*) calculation with five quantiles, as listed in Tables 1 and 2.

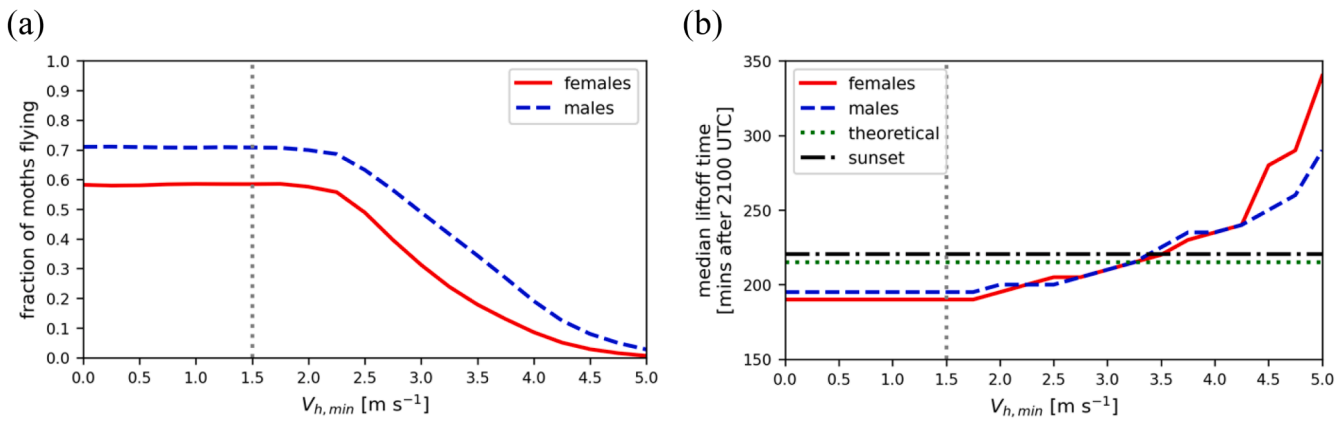

Fig. 5. Effect of variation in the liftoff minimum horizontal windspeed parameter $V_{h,\min}$ on 15–16 July 2013 simulations of SBW moth dispersal: (a) liftoff rates; (b) median liftoff times, compared to the unmodulated circadian rhythm of flight activity (green horizontal line) and relative to sunset (black horizontal line). In each plot, SBW females are represented by the solid red line, SBW males by the dashed blue line, and $V_{h,\min} = 1.5$ m s^{-1} by the dotted gray line.

et al., 2019b). At higher values of $V_{h.\min}$ the median timing of liftoff for those moths that fly (considering the liftoff rates in Fig. 5a) gets progressively later, crossing the time of median theoretical liftoff and the sunset time at about $V_{h.\min} = 3.5$ m s^{-1}. For that relatively restrictive liftoff condition, only about 25 % of the simulated moths fly at all, and the flight fraction falls to near zero with higher values of $V_{h.\min}$.

4.2. Conversion of wingbeat to flight speed, ε

The wingbeat conversion parameter ε affects the speed of moth ascent through the boundary layer and the ground-relative flight speed of moths once they have lifted off, with lower flight speeds at greater values of ε (Fig. 6a). We note that this effect is quasi-linear and that females consistently have greater flight speeds than males. The flight speed, combined with the moth's weight, represents the power of the moth to reach a greater flight altitude and overall dispersal distance.

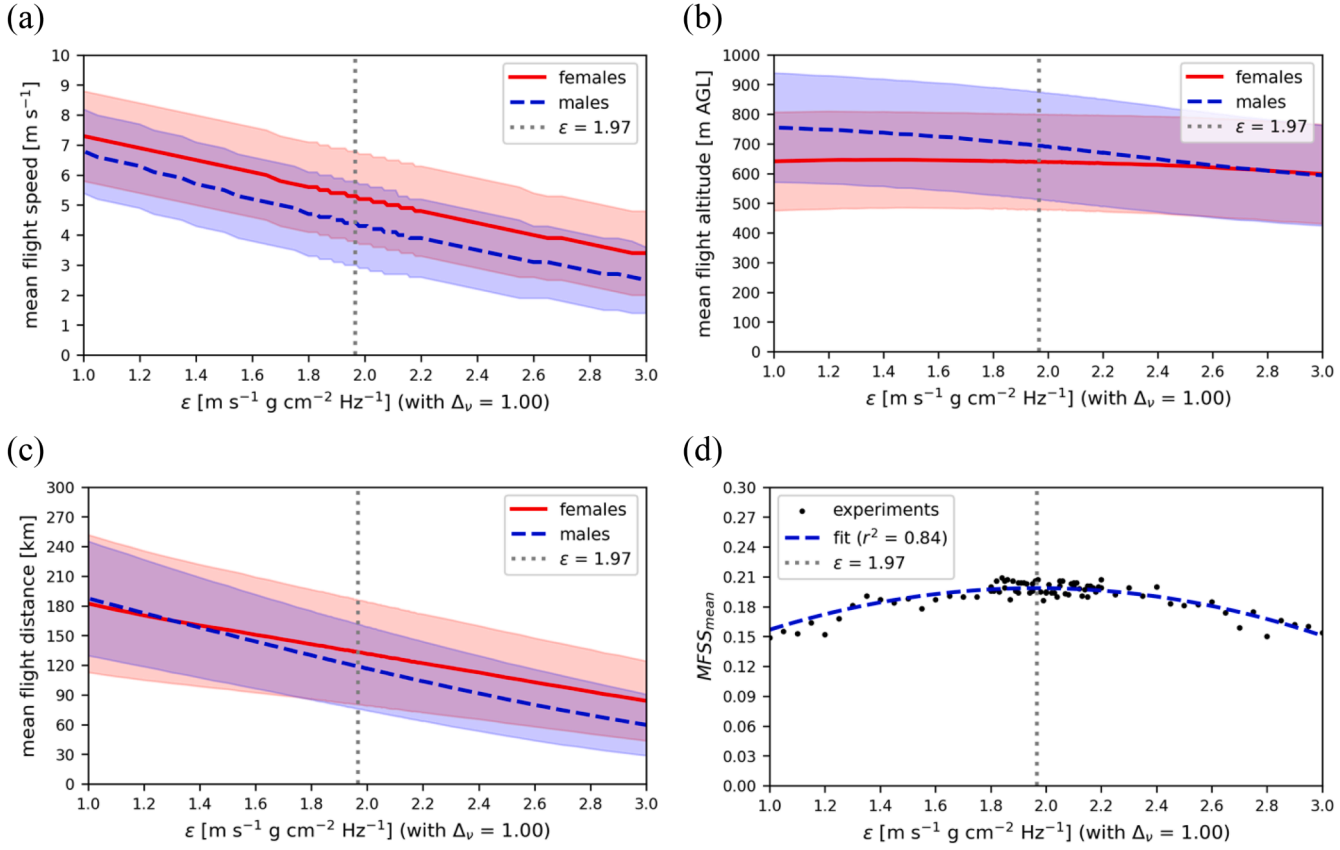

Fig. 6. Effect of variation in the wingbeat-to-flight-speed coefficient ε on 15–16 July 2013 simulations of SBW moth dispersal, with $V_{h,\min} = 1.5$ m s^{-1} and $\Delta_\nu = 1.0$: (a) mean ground-relative flight speed; (b) mean flight altitude; and (c) mean flight distance; (d) the simulation $MFSS_{mean}$ within the northwest quadrant of the XAM radar coverage area (dots: individual simulation results; blue dashed line: quadratic least-squares fit, $r^2 = 0.84$). In (a)–(c), SBW females are represented by the solid red line and SBW males by the dashed blue line. Shaded regions represent the mean quantity ± 1 standard deviation across the collected simulations. The optimum value $\varepsilon = 1.97$ m s^{-1} g cm^{-2} Hz^{-1} is represented by the dotted gray (vertical) line in all plots.

Males are typically lighter than females and, thus, often reach higher flight altitudes. Our results show that variations in the value of ε have a far greater effect on SBW males, whose overall flight altitude decreases with rising values of ε, and very little effect on the flight altitude of females, which remain at consistently lower altitudes than the males despite greater flight speeds (Fig. 6b). Together, flight speed and altitude combine to affect the overall flight distance, which diminishes more quickly with higher values of ε for males than for females (Fig. 6c). The parameter ε has no effect on the timing or proportion of moths lifting off from the forest canopy, but it has a profound effect on the density and motion of the moths in the modeled airspace. Based on the calculated *MFSS* using simulated moth concentrations and radar reflectivity throughout the night of 15–16 July, simplified with a quadratic curve fitted to the collection of individual experiment results using $\Delta_\nu = 1.0$ (Fig. 6d), we selected the optimal value of $\varepsilon = 1.97$ m s^{-1} g cm^{-2} Hz^{-1}. In Part 1, we had selected $\varepsilon = 1.58$ m s^{-1} g cm^{-2} Hz^{-1} as an optimal value from a limited exploration of the parameter space. In our expanded experiments covering a wider value range, we found that the value selected in Part 1 was a local maximum in the *MFSS* results and that the higher value selected here produced better *MFSS* results. However, the difference in *MFSS* values between these two results is small enough that it does not invalidate any of the qualitative assessments reported in Part 1.

4.3. Conserving energy in flight, Δ_ν

Because the energy conservation parameter Δ_ν does not apply immediately upon liftoff, variations in Δ_ν do not affect the fraction or timing of moths lifting off for dispersal flights. We found that higher values of Δ_ν led to slower SBW moth flight speeds (Fig. 7a). The mean flight altitude is slightly greater for SBW males than females and, consistent with attempts to conserve energy by reducing wingbeat frequency, diminishes with lower values of Δ_ν (Fig. 7b). We found that this reduction appears non-linear and is reflected in the mean flight distances that diminish far more quickly for SBW females than for males (Fig. 7c), enough that the slightly greater flight distances exhibited by SBW females at $\Delta_\nu = 1.0$ (see also Fig. 6c) are offset completely when values of $\Delta_\nu < 0.9$ are used.

The calculated *MFSS* between modeled moth concentrations and radar reflectivity through the night over the range of Δ_ν experiments (Fig. 7d) suggests that the optimal value of the energy conservation parameter, using $\varepsilon = 1.97$ m s^{-1} g cm^{-2} Hz^{-1}, could be $\Delta_\nu = 0.99$. However, we found in two-parameter simulations (below) that $\Delta_\nu = 1.0$ still offers a better overall outcome. Though our simulation results at $\Delta_\nu = 1.0$ do not match the radar observations perfectly ($MFSS_{mean} = 0.182$, $MFSS_{max} = 0.343$), the overall patterns of moth dispersal represented by the timing and location of moth concentrations in our simulations using $\Delta_\nu = 1.0$ are far closer to the observations than at lower values of Δ_ν.

4.4. Interaction between Δ_ν and ε

We have demonstrated through these simulations that variations in both the wingbeat conversion parameter ε and the energy conservation parameter Δ_ν can strongly affect moth flight speed, altitude, and distance. To look at possible interaction effects between ε and Δ_ν we performed numerous experiments covering the parameter spaces for these two as listed in Table 1. The quadratic curves fitted to the resulting *MFSS* values from each set of experiments (Fig. 8, *cf.* Fig. 6d) show decreases in

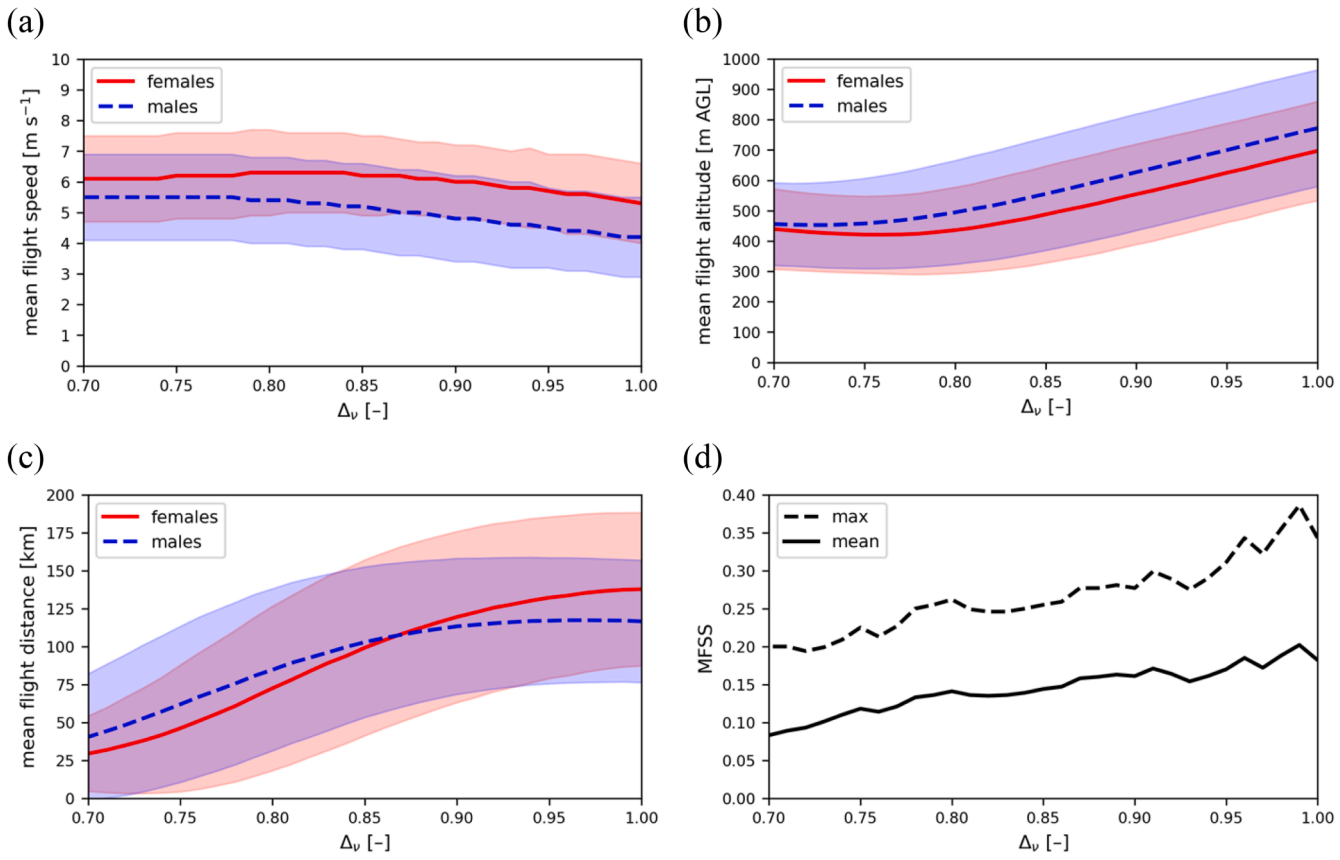

Fig. 7. Effect of variation in the unitless energy conservation parameter Δ_ν on 15–16 July 2013 simulations of SBW moth dispersal, with $V_{h,\min} = 1.5$ m s^{-1} and $\varepsilon = 1.97$ m s^{-1} g cm^{-2} Hz^{-1}: (a) mean ground-relative flight speed; (b) mean flight altitude; (c) mean flight distance; (d) the simulation $MFSS_{mean}$ within the northwest quadrant of the XAM radar coverage area. In (a)–(c), SBW females are represented by the solid red line, SBW males by the dashed blue line, and shaded regions represent the mean ± 1 standard deviation across the collected simulations.

Table 1
SBW–pyATM moth flight parameters explored here.

Symbol [units]	Parameter description	Expected range	Tested range and increment
$V_{h,\min}$ [m s^{-1}]	Minimum wind speed for liftoff	1.00 – 2.00	0.00 – 5.00 @ 0.25
ε [m s^{-1} g cm^{-2} Hz^{-1}]	Conversion of wingbeat to flight speed	1.00 – 1.50	0.80 – 3.00 @ 0.05 and 0.01
Δ_ν [unitless]	Energy conservation in flight	0.90 – 1.00	0.70 – 1.00 @ 0.01

Table 2
Example quantiles and areas to support calculating the Modified Fractions Skill Score (*MFSS*) for the input fields shown in Fig. 2.

Quantile	Radar value range	Radar # of pixels in range	Simulation value range	Simulation # of pixels in range
1	0.1 – 8	1808 px	0.1 – 8	1020 px
2	8.1 – 16	1416 px	8.1 – 16	784 px
3	16.1 – 24	996 px	16.1 – 24	568 px
4	24.1 – 32	600 px	24.1 – 32	328 px
5	32.1 – 40	193 px	32.1 – 40	109 px
Total		5013 px		2809 px

overall simulation accuracy with the deviation of ε from an optimum in the range $1.8 < \varepsilon < 2.1$ m s^{-1} g cm^{-2} Hz^{-1} and with values of $\Delta_\nu < 1.0$. There is a large difference in the optimum value of ε when the value of Δ_ν is decreased from 1.0 to 0.99, but then there is little variation in the optimum value of ε in the range $0.95 \leq \Delta_\nu \leq 0.99$. For $\Delta_\nu = 0.9$, 0.8, and 0.7, the optimum value of ε continues to decrease with Δ_ν. Given the overall maximum *MFSS* value obtained at $\Delta_\nu = 1.0$ and $\varepsilon = 1.97$ m s^{-1} g cm^{-2} Hz^{-1} (Fig. 8), we have elected to use those values in our validation flight experiment.

4.5. Calibration results from 15 to 16 July 2013 applied to 14–15 July 2013

Finally, we present a summary of calibrated simulations of SBW moth dispersal for the night of 15–16 July 2013 using the optimum parameter values $V_{h,\min} = 1.5$ m s^{-1}, $\varepsilon = 1.97$ m s^{-1} g cm^{-2} Hz^{-1}, and $\Delta_\nu = 1.0$, and the results using those optimum parameter values for simulations of SBW moth dispersal on the previous night, 14–15 July 2013. The weather conditions for each night that were presented in Part 1 and their differences across the two nights are highly relevant to the discussion of results here. Simulated flight trajectories for each night using the radar-calibrated parameters are shown in Fig. 9 and the overall flight statistics are listed in Table 4.

For both nights, the start of liftoff is similar in the two sexes (Fig. 10a, b), about 15–30 min earlier than expected from the circadian model (Régnière et al., 2019b) using WRF-derived surface temperatures. Those WRF simulations indicated that near-surface temperatures cooled more quickly on the night of 14 July than on the night of 15 July, as reflected in the stretched-out curve for the timing of later SBW liftoffs on the night of 14 July and leading to the later mean liftoff time closer to sunset on that night (Table 4). With more rapid cooling near the surface on the night of 14 July, warm boundary layer air was likely forced higher, leading to mean flight altitudes ~150 m higher for both SBW males and females than on the night of 15 July (Figs. 10c, d). A greater mean wind speed on the night of 14 July led to similarly greater mean flight speeds

Table 3
Example calculation of the Modified Fractions Skill Score (*MFSS*) for the given input fields (Fig. 2, Table 1) and calculated quantile areas shown in Fig. 3.

Quantile range	Radar value range	Radar # of pixels in range	Simulation value range	Simulation # of pixels in range	Intersection # of pixels	Union # of pixels	$MFSS_q$
1 – 5	0.1 – 40	5013 px	0.1 – 40	2809 px	1852 px	5970 px	0.310
2 – 5	8.1 – 40	3205 px	8.1 – 40	1789 px	915 px	4079 px	0.224
3 – 5	16.1 – 40	1789 px	16.1 – 40	1005 px	281 px	2513 px	0.112
4 – 5	24.1 – 40	793 px	24.1 – 40	437 px	0 px	1230 px	0.000
5	32.1 – 40	193 px	32.1 – 40	109 px	0 px	302 px	0.000
Overall					3048 px	14094 px	**0.216**

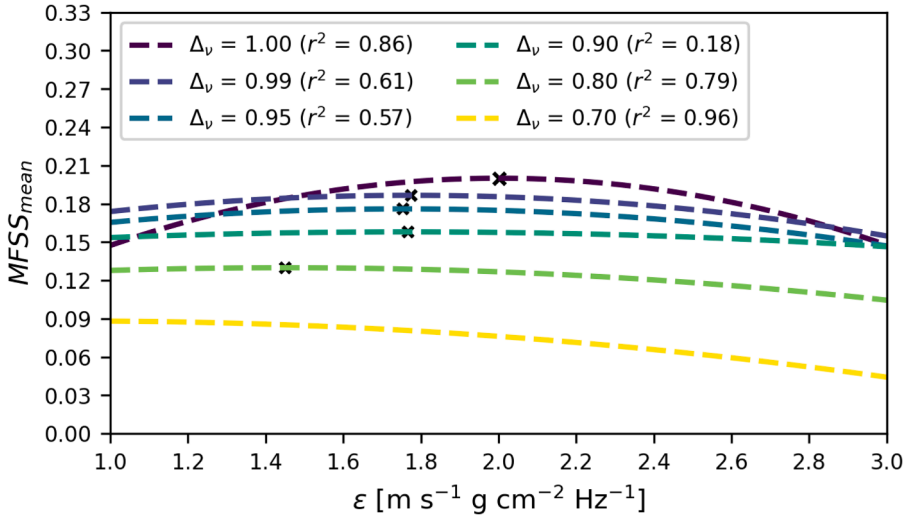

Fig. 8. Effects of variations in both the wingbeat-to-flight-speed coefficient ε and the energy conservation parameter Δ_ν on experimental $MFSS_{mean}$ results for 15–16 July 2013 simulations of SBW moth dispersal, with $V_{h,\min} = 1.5$ m s^{-1}. The overall maximum value of $MFSS_{mean}$ (marked by the × on each fitted curve) occurs at $\varepsilon = 1.97$ m s^{-1} g cm^{-2} Hz^{-1} and $\Delta_\nu = 1.0$.

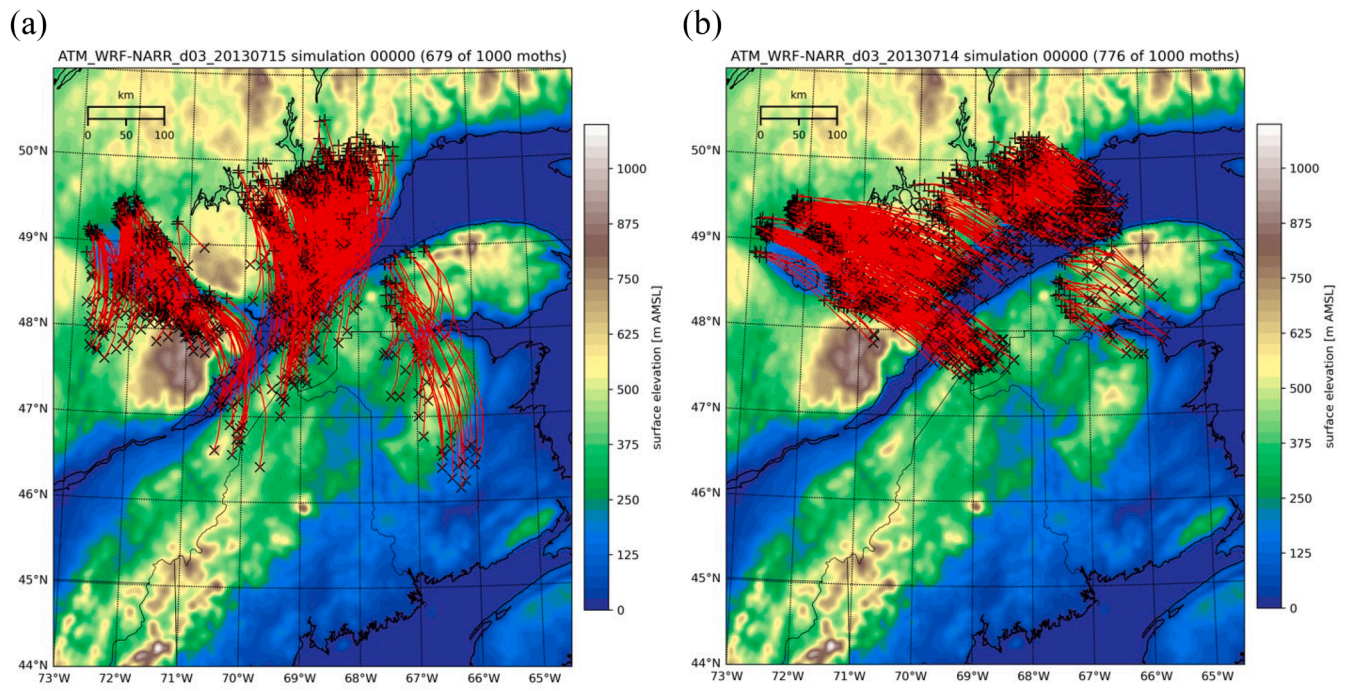

Fig. 9. Simulated flight trajectories for (a) 15–16 July 2013 and (b) 14–15 July 2013 simulations of SBW moth dispersal using $V_{h,\min} = 1.5$ m s^{-1}, $\varepsilon = 1.97$ m s^{-1} g cm^{-2} Hz^{-1}, and $\Delta_\nu = 1.0$. Liftoff locations are indicated by + and landing locations by ×.

for both SBW males and females for that night (Table 4). Combined with higher flight altitude, these factors led to generally greater flight distances on the night of 14 July by ~25 km for SBW males and ~50 km for females (Fig. 10e, F), despite similar flight durations across both nights (Table 4).

As shown in Part 1, our simulated flight trajectories are reasonably consistent with the XAM radar observations over both nights in this study. Calculated *MFSS* values for the night of 15–16 July show good agreement between the calibrated spatiotemporal moth densities and the radar observation time series (Fig. 11a). The start of the mass dispersal flight in the hour prior to sunset (Fig. 10a) is reflected in the rise of *MFSS* values around that time to a level that only improved through the night, indicating that our simulation results became more like the radar observations over time. This similarity peaked ~2 h before sunrise, after which time the radar signal showed a rapid end to the dispersal flight. The drop to *MFSS* = 0 near sunrise is not because our simulations diverge significantly from the radar observations but because the signs of moth flight in both information sources disappear in a matter of minutes around that time, presumably due to the SBW moths landing as assumed in the pyATM model. Using the calibrated parameters from the 15–16 July simulations, our simulations of SBW moth dispersal flights on the night of 14–15 July 2013 showed similar consistency with radar observations (Fig. 11b). Though the overall similarity to radar observations for this event did not ultimately reach such a high level as for the calibration experiments, the later start of flight activity (Fig. 10b) is appropriately reflected in suppressed *MFSS* values until ~30 min after sunset. The similarities between simulated and radar-observed moth densities then began to grow until reaching a plateau around 3 h before sunrise and then dropped off quickly after sunrise, as for the 15–16 July calibration experiments.

5. Discussion

We have used weather radar observations of insect mass dispersal events over moderate scales, ~20–200 km, to improve the representation of individual behavior within a modeled SBW flight event, improving the validity of the simulated event outcomes. Our results, based primarily on the application of meteorological forecast validation methods to comparisons between modeled flight trajectories and weather radar data, reinforce our confidence in the flight model formulation as presented in Part 1 and our identification here of the salient flight parameters that remained uncertain and needed further investigation. We have improved the selected value for the wingbeat conversion parameter ε following numerous additional simulations that explored the value space of that parameter alone and through interaction with the energy conservation parameter Δ_ν. At the same time, our prior assumption that conserving energy may not be a priority for the SBW during dispersal flight seems to have held, with numerous experiments suggesting that the optimum value is $\Delta_\nu = 1.0$ as used in Part 1.

Long-distance weather-driven dispersal, the descriptive goal of our model, typically occurs well above the surface and almost exclusively outside the range at which individual moth behavior can be directly observed. Near the ground and below the forest canopy, where winds are often light, the SBW engages in directed flight for males to find a mate and for females to find a suitable host tree for egg deposition (Sanders, 1983, 1987). In stronger winds several hundred meters above the forest canopy, it seems far less likely that the moths can control their own flight direction, and much more likely that their principal energy expenditure is simply fighting gravity to remain aloft as long as possible. For physical consistency between our model and the available radar observations, we developed a conceptual picture of SBW in-flight orientation in which the moth's *directed* (forward, goal-oriented) flight is upward, helping to control its altitude according to the boundary layer temperature profile, and its consequential *wind-relative* motion is essentially backward so that its overall *ground-relative* motion is slower than the wind but in the same direction. Qualitatively in Part 1 and quantitatively here, we found this conceptual model to be consistent with the available radar observations: we noticed that the weather radar echoes (representing masses of moths in flight) moved in the same direction as the wind but not as fast as the model-provided winds would have suggested, *contra* Sturtevant et al. (2013). We do not contend that the SBW moths attempt to fly into the wind, but rather that their orientation is downwind and "nose-up," and that SBW moths are thus carried along in *semi-passive* flight. Our somewhat counterintuitive

Table 4
Calibration and validation results from SBW dispersal simulations for the nights of 15–16 July and 14–15 July 2013, respectively. Values with ranges are given as the mean ± 1 standard deviation; LDT = local daylight time (UTC – 4 h); AGL = altitude above ground level.

Simulation flight indicator	15–16 July 2013 (calibration)	14–15 July 2013 (validation)
Fraction of moths flying		
overall	67.2 %	79.0 %
females	63.8 %	76.4 %
males	71.4 %	83.7 %
Mean overall flight start time	20:27 LDT ± 54 min	21:03 LDT ± 78 min
Sunset time at XAM	20:28 LDT	20:29 LDT
Mean wind speed	9.1 m s^{-1}	9.2 m s^{-1}
Ground-relative flight speed		
overall	4.6 ± 1.4 m s^{-1}	4.7 ± 1.6 m s^{-1}
females	5.3 ± 1.3 m s^{-1}	5.6 ± 1.2 m s^{-1}
males	4.2 ± 1.3 m s^{-1}	4.1 ± 1.5 m s^{-1}
Mean flight altitude		
overall	743 ± 185 m AGL	874 ± 205 m AGL
females	698 ± 162 m AGL	821 ± 193 m AGL
males	772 ± 193 m AGL	908 ± 205 m AGL
Max flight altitude		
overall	1005 ± 201 m AGL	1162 ± 203 m AGL
females	979 ± 199 m AGL	1126 ± 199 m AGL
males	1022 ± 200 m AGL	1185 ± 203 m AGL
Flight duration		
overall	457 ± 109 min (max 721 min)	460 ± 90 min (max 714 min)
females	436 ± 123 min (max 721 min)	457 ± 91 min (max 703 min)
males	470 ± 96 min (max 711 min)	462 ± 89 min (max 714 min)
Flight distance		
overall	125 ± 46 km (max 339 km)	128 ± 45 km (max 262 km)
females	138 ± 50 km (max 339 km)	153 ± 38 km (max 262 km)
males	117 ± 40 km (max 318 km)	112 ± 41 km (max 262 km)
MFSS results		
mean	0.196	0.057
max	0.378	0.154

proposition, that the SBW moths fly slower than the wind but still travel downstream, is supported by comparisons between input WRF wind fields, our modeling results, and the radar observations. Nevertheless, this conceptual model has raised some questions regarding physical mechanisms that we address here through analogies with studies of hawkmoth (*Manduca sexta*) flight behavior by Willmott and Ellington (1997a, b). The moth's dispersal by lateral translation is then a function of how long it can flap its wings to remain aloft given ambient temperature, precipitation, and vertical wind conditions. In modeling terms, these conditions are encoded in the ability of the moth to lift off (Régnière et al., 2019b), the dependence of the moth's wingbeat on the ambient temperature (Régnière et al., 2019a), and the conditions under which the moth descends for landing. Our findings suggest that the SBW moth may not be as strong a flier as previously thought (Greenbank et al., 1980; Sturtevant et al., 2013), with significant consequences for the geographic area reachable from an existing SBW outbreak location via wind-driven dispersal flight.

5.1. Caveats

There are a few caveats to the findings presented above, some due to our modeling procedure and others to remaining uncertainties in the system that we are attempting to reproduce in our modeling framework. Finding a minimum wind speed for liftoff was relatively simple, given no discernible variability among simulations with values of $V_{h,\min}$ below the selected threshold, but large variability among simulations with values above that threshold. Since we do not explicitly treat low-level SBW flight activities in calm conditions and under their own power, our dispersal flight modeling outcomes are consistent with historical observations that moth liftoff and subsequent flight are less likely in calm near-surface conditions. To some degree, these simulations helped us better define "calm" as the term was used by Greenbank et al. (1980) when describing SBW liftoff behavior. Our simulations with higher values of $V_{h,\min}$ showed that stricter conditions, such as $V_h \geq 4.0$ m s^{-1}, were rarely met during the night of 15–16 July 2013 and that few moths lifted off through the night under such restrictions. The thermal stratification of the boundary layer, which typically changes through the night, can play a significant role in this occurrence: in a more stable atmospheric boundary layer that can be established well after sunset, stronger winds originating near the top of the boundary layer are less likely to propagate all the way to the surface and cause wind gusts there (Lemone et al., 1999; Sun et al., 2004), leaving relatively cool and calm conditions in the forest canopy where SBW moths attempt to lift off. Those conditions may become too calm in such cases, with wind speeds falling below our threshold requirement for liftoff. The moth cannot know of, much less reach, the potentially ideal dispersal flight conditions occurring only a few hundred meters above the forest canopy.

On the other hand, procedures to find the optimum values for the wingbeat conversion coefficient ε and the energy conservation coefficient Δ_ν were complex, in part because their use in the model is tied to both vertical *and* horizontal motion, and in part because the radar data cannot show us individual moths, only the collective behavior of moths in a remotely-sensed volume of atmosphere, and generally only the horizontal motion of the moths in that volume. The *MFSS* metric is general enough to allow large variability in the overall calculation results, prompting us to fit a quadratic function to our results (Fig. 6d) to estimate an optimum value for the wingbeat conversion coefficient ε. We also demonstrated that the Δ_ν value interacts with the flight speed coefficient ε. While variations of Δ_ν significantly affected simulation *MFSS* values, there seemed to be consistent effects on ε, with generally lower optimum values of ε found as Δ_ν decreased.

Using the values of the parameters that we calibrated on the night of 15–16 July to simulate the dispersal flights on the night of 14–15 July led to reasonable results: as shown in Part 1, moth flights on the earlier night were physically consistent with the greater wind speeds (see Table 4) and different wind directions that our WRF results demonstrated for that night. Obtaining physically realistic moth flight trajectories over complex terrain amid varying winds and temperature profiles was among our chief concerns when designing this model, so it is encouraging to find that flight parameters determined both empirically and numerically are transferable across simulations on different nights with significantly different weather conditions.

5.2. Remaining sources of uncertainty

Overall, our remaining sources of uncertainty in the model formulation are related to (1) near-ground behavior at liftoff and landing, (2) homogeneity, and (3) the ever-present problems of choice, by which we mean behaviors that occur in response to stimuli and behavioral pathways that are beyond our current understanding, realizing that we still know little regarding neurological capabilities of insects (Nityananda, 2016). Our work has thus far focused on above-canopy, wind-driven SBW dispersal; a separate examination of SBW liftoff and flight behavior in relatively calm conditions may reveal significant daytime redistribution of moths below and near the level of the forest canopy over small to moderate distances. Depending on where the moths gather amid host trees and surface topography (Dickison, 1990; Pedgley et al., 1990), and their resulting exposure to conditions favoring wind-driven above-canopy dispersal during the evening and night, this mode of daytime spatial redistribution could lead to lesser or greater numbers of nighttime dispersal flights. These are aspects of SBW behavior and movement that our model does not yet include. We include several mechanisms for moth landing such as cold, rain, and sunrise, but there may be other

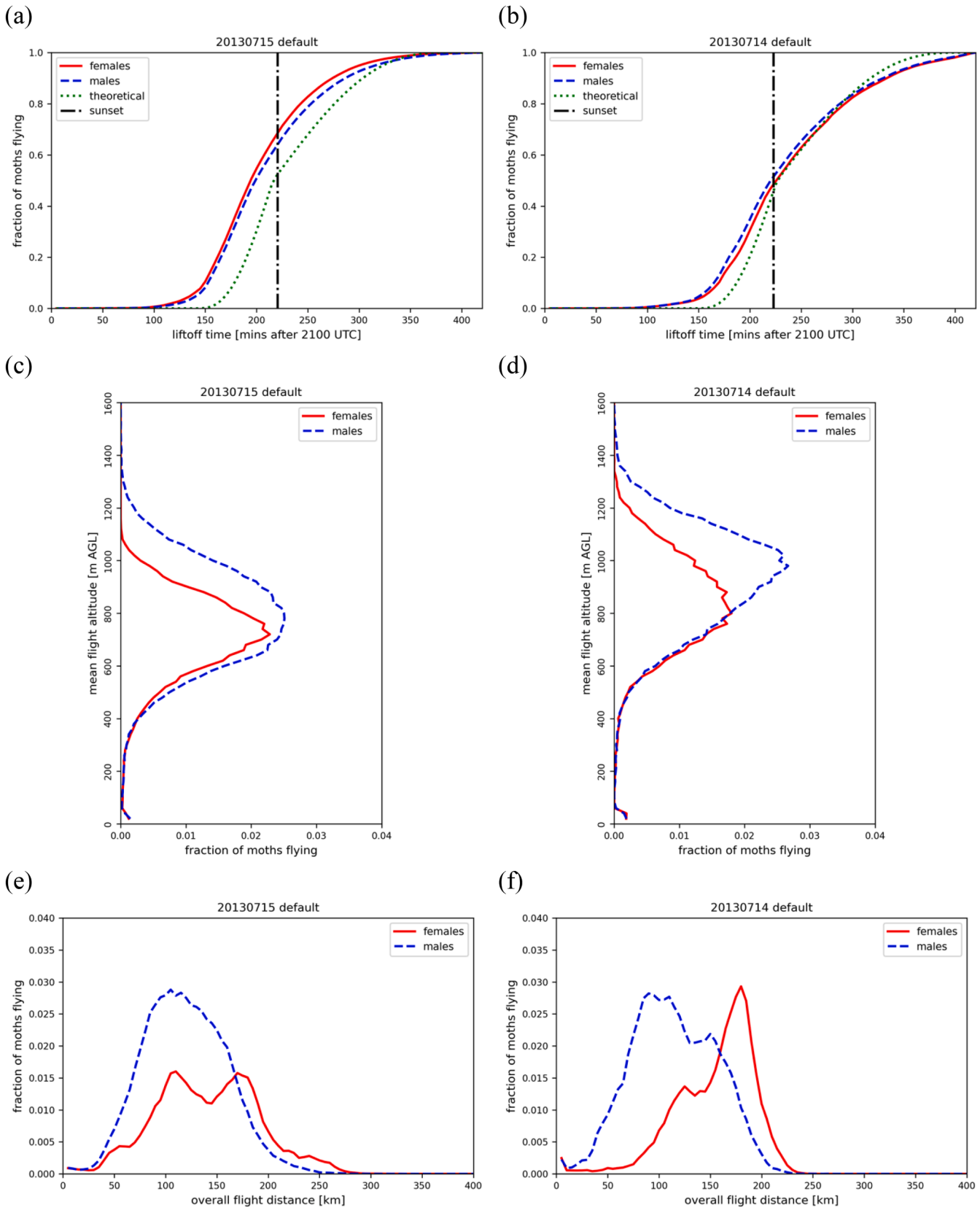

Fig. 10. Summary of 15–16 July 2013 (left column) and 14–15 July 2013 (right column) simulations of SBW moth dispersal using $V_{h,\min} = 1.5$ m s^{-1}, $\varepsilon = 1.97$ m s^{-1} g cm^{-2} Hz^{-1}, and $\Delta_\nu = 1.0$: (a)–(b) liftoff times; (c)–(d) mean flight altitude; (e)–(f) overall flight distance. In each plot, SBW females are represented by the solid red line and SBW males by the dashed blue line.

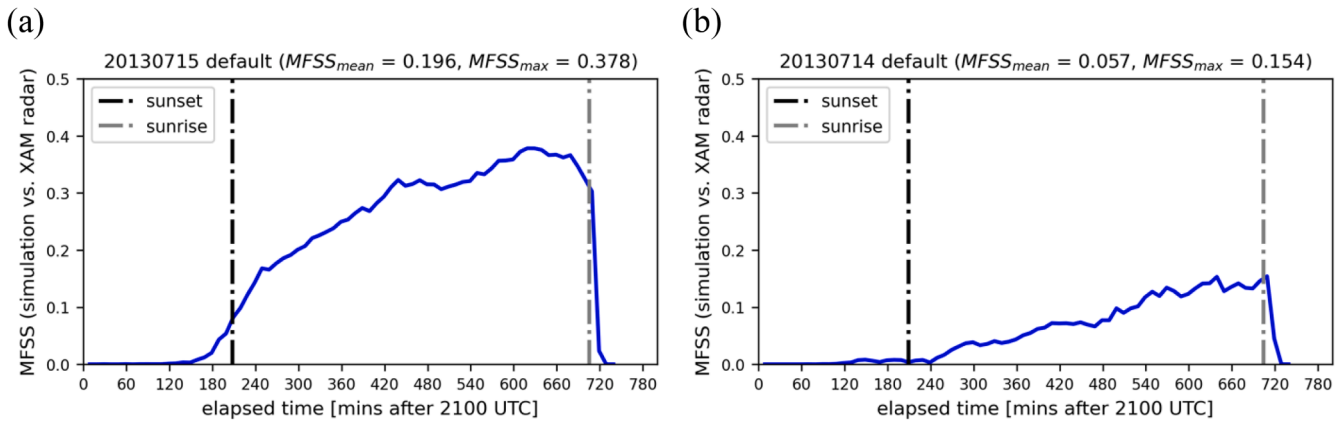

Fig. 11. Results for SBW flight simulations using $V_{h,\min} = 1.5$ m s^{-1}, $\varepsilon = 1.97$ m s^{-1} g cm^{-2} Hz^{-1}, and $\Delta_\nu = 1.0$. (a) *MFSS* during the calibration simulations on 15–16 July 2013; (b) *MFSS* during the validation simulations on 14–15 July 2013.

factors that prompt moths to land, such as exhaustion (available energy) or external stimuli (*e.g.*, visual, olfactory) that are not yet represented in our model.

Unfortunately, weather radar observations cannot help us better understand flight behavior close to the ground because of interference by topography and the forest itself. We are loath to place too many rules and restrictions on modeled liftoff behavior, in part because we cannot think for the moth or anthropomorphize its decision process. However, there remains the possibility that immediate flight factors such as wing wear (Rhainds and Brodersen, 2012; Rhainds, 2015; Rajabi et al., 2020; Korkmaz et al., 2023) could change the value of the wingbeat conversion parameter ε or that the parameter Δ_ν could be repurposed to account for aging, fatigue, and diminished energy reserves. Though both parameters in our model arose from our conceptual approach to individual moth flight activity, more empirical research is needed to link these numerical parameters more closely to the actual physical processes of moth flight in real conditions where individual flight activity is often difficult to observe directly.

Second, we assume homogeneity of our model flight parameters across the population of simulated SBW moths. The moths themselves are not homogeneous: each is assigned a mass and wing size according to the distributions of those morphological parameters for its sex (see Régnière et al., 2019a), but it remains possible that many moth characteristics could vary with larval feeding, mating status, adult age, and energy expenditure over prior flights. These uncertainties could be addressed with additional model complexity, stochasticity in the assignment of individual flight parameters, and more simulation replicates, but we do not yet know how well those approximations would represent behavioral variability in real moths, which only additional observations can tell us.

Without anthropomorphizing SBW moth behavior, we must eventually address issues of choice. We have already stated that our model does not include communication between moths, so behavioral organization is eliminated, and all the recognizable patterns that we see in our results are thus emergent properties of the individual-based system. But for the SBW moth, are individual take-off responses adaptive in terms of the risk of liftoff and flight in strong winds? Are there minimum dispersal distances or durations leading to a greater likelihood of outbreak propagation? What are the conditions under which moths lift off again on the same night or a subsequent night, conditions permitting? Do SBW moths choose when and where to land? And finally, do some moths choose *not* to fly, even when the conditions are favorable?

5.3. Demographic sorting

All the above questions and related uncertainties contribute to the overall dispersal of the SBW moths, including their survival in flight, and can have significant influences on the resulting spatial patterns of egg deposition, transfer of fecundity across regions, and the role of dispersed males in alleviating mating failure in SBW subpopulations at landing locations (Contarini et al., 2009; Rhainds, 2010; Régnière et al., 2013). In Part 1, we proposed that "the two sexes are unlikely to perform their respective roles in the same locations and at the same time over the course of the dispersal season." The work presented here supports that inference. As indicated by differing flight altitudes and distances, adult SBW females and males do not systematically disperse to the same locations each night. The forward speed of the SBW adult moth during dispersal is critical to flight trajectory calculations, but so is the ability of the moth to remain at an optimum flight altitude where the temperature and wind can assist such migration. This is especially the case for gravid females, with greater body weight and thus lower flight strength, and yet we find that females often travel somewhat farther than males during a night of dispersal (Figs. 6c and 7d). This, along with males generally flying higher than females (Figs. 6b and 7c) such that males' flight paths may be less affected by terrain, leads to what we have termed *demographic sorting*: SBW males apparently disperse over shorter distances from their natal sites, and their further utility in reproduction depends entirely on landing in a location where unmated females have recently emerged; mated SBW females seem to disperse over greater distances, and their utility in reproduction continues without further need for the males wherever they find suitable host species around their landing sites. Heavier moths, typically females but also some males, likely remain closer to the ground during flight, finding valleys and low mountain passes that could be overlooked by lighter, higher fliers including most males. Age and energy expenditure could also play a role: older moths are more likely to have flown at least once before on a prior night, and so might be expected to behave more like heavier moths as their energy reserves are diminished. Older males may still be useful to the mating process, provided they land where emergent females are available, while older females are more likely to have already laid eggs on more occasions and have few remaining eggs to deposit at their final landing site.

The values of the flight parameters ε and Δ_ν thus have significant effects on the simulated spatial distribution of migration landing sites and egg deposition, making both parameters highly important to further study and the overall application of empirical observations and individual-based modeling principles to the SBW dispersal system. The individual roles of SBW females and males in reproduction, supporting the maintenance and expansion of an SBW outbreak area, will likely be carried out in different places. We provided example results in Part 1 showing the simulated dispersal areas of males and gravid females on each of the two nights examined here. With a better-calibrated model, we can expand on those earlier results with examinations of a sequence of dispersal events, over an entire summer if possible, and to assess the

roles of individual SBW moth dispersal flight behavior on emergent, landscape-wide SBW outbreak dynamics. Validation of such results will then extend to the application of ground-based traps, aerial surveys, and remote sensing methods where adequate data are available.

6. Conclusion

In the growing field of radar aeroecology, individual-based models of wind-driven insect dispersal have a detailed and informative data source with which the modeled, aggregate flight behavior of the insects may be calibrated and refined. Radar data available during SBW dispersal flights in southern Quebec on the nights of 14–16 July 2013 have provided valuable comparisons for us to perform numerous experiments in individual-based flight modeling across a range of parameter values, and thus calibrate three of the less-certain parameters in our model formulation. These calibration exercises led to realistic results on both nights examined here.

Our results show that long-distance SBW dispersal flights are not only possible but likely, with the majority of SBW moths traveling farther than 100 km in all our simulations for these two nights. We anticipate, by extending our simulation experiments to other dates, the ability to indicate periods during which more long-distance flights are likely under the available weather conditions. As we further develop solutions to the caveats and remaining uncertainties expressed below, we look forward to validating our modeled dispersal results against still more radar observations and additional information sources, from those on the small-scale such as ground-based light- and pheromone-trap capture records (Rhainds and Kettela, 2014; Rhainds, 2015; Rhainds et al., 2019, 2022) to large-scale assessments of defoliation as observed in aerial surveys (MacLean and MacKinnon, 1996; Taylor and MacLean, 2008) and in remote sensing analyses (Rahimzadeh-Bajgiran et al., 2018).

Despite frequent emphasis on the mechanics of long-distance insect dispersal (Sturtevant et al., 2013; Chapman et al., 2015; Dargent et al., 2023; Gandiaga and James, 2023), especially as a potential driver of spatial synchrony in insect outbreak cycles (Williams and Liebhold, 2000; Peltonen et al., 2002; Bouchard et al., 2018; Larroque et al., 2019), shorter flights (*e.g.*, less than ~20 km) are more consistent with the slower, diffusion-like spread of the SBW population in affected areas (Bouchard and Auger, 2014). Both long-distance dispersal of SBW moths in favorable weather conditions and short-range reorganization of SBW in daily below-canopy activity (including mating) must be considered in the investigation and management of SBW outbreak behavior. As discussed in Part 1 and in this work, spatiotemporal patterns of SBW liftoff, landing, and egg deposition are ultimately sensitive to flight dynamics. The overall emergent patterns of dispersal and its effects on outbreak spread may show evidence of demographic sorting between males and females on a nightly basis, made more complex by multiple dispersal episodes over several weeks of the summer season. Landing followed by host- and mate-seeking behavior at the end of a dispersal flight is not yet described in our individual-based model. We are motivated to acquire more evidence that will improve that part of our flight model and bring it closer to real SBW behavior.

We are encouraged toward further work with this mass dispersal flight model, from validation (and perhaps re-calibration) against additional radar data during other dispersal events, to expansion of our modeling efforts to full dispersal seasons, each night building on the previous results for a realistic estimate of the overall regional redistribution of the SBW population that occurs by the end of the summer. Validation efforts at that stage of model application will bring together a much wider variety of data sources and methods than we have undertaken thus far.

Our model calibration procedure and results suggest that other efforts to simulate insect dispersal using individual-based model formulations could benefit from detailed analyses of uncertain model parameters and their effects on the mass of dispersing insects as viewed in weather (or other specialized) radar observations. Using radar observations, the emergent and aggregate behavior of the insect mass can be tracked at a scale far different from the focus on the individual insect in the model formulation. This may be especially useful in situations where dispersing forest and agricultural pests are observed regularly by weather radar in the summer months, with a wealth of radar observations available to anchor a parameter exploration and calibration effort.

Code availability

Updated SBW–pyATM model code, sample datasets, and supplemental animations of simulation results are available at https://github.com/megarcia/SBW-pyATM. Python scripts and Jupyter Notebook examples for processing simulation ensembles, calculating the *MFSS* metric, and generating the figures in this paper have been added to that project repository alongside the resources related to Part 1 of this series.

CRediT authorship contribution statement

Matthew Garcia: Writing – review & editing, Writing – original draft, Visualization, Validation, Software, Resources, Methodology, Investigation, Formal analysis, Data curation, Conceptualization. **Brian R. Sturtevant:** Writing – review & editing, Supervision, Resources, Methodology, Funding acquisition, Conceptualization. **Yan Boulanger:** Writing – review & editing, Supervision, Methodology, Data curation. **Jacques Régnière:** Writing – review & editing, Writing – original draft, Supervision, Resources, Project administration, Methodology, Investigation, Funding acquisition, Conceptualization.

Declaration of competing interest

The authors declare that they have no known competing financial interests or personal relationships that could have appeared to influence the work reported in this paper.

Data availability

Data will be made available on request.

Acknowledgments

We acknowledge Barry Cooke of the Canadian Forest Service and Jay Charney of the U.S. Forest Service for their contributions to the early stages of this project, and Rémi Saint-Amant of the Canadian Forest Service for discussions and technical contributions throughout this project. We thank Frédéric Fabry at the J.S. Marshall Observatory, McGill University, for processing the radar data used here. We also thank Philip Townsend and the EnSpec Lab at UW–Madison for logistical support, helpful feedback, and discussions throughout this work.

Funding and additional resources directly supporting this work were provided by the U.S. Endowment for Forestry and Communities, the U.S.–Canadian Forest Health Initiative, the Northern Research Station of the U.S. Forest Service in the U.S. Department of Agriculture, the Healthy Forest Partnership Early Intervention Strategy financed by the Federal Government of Canada in partnership with participating Provinces and forest industry, and the Department of Forest and Wildlife Ecology in the College of Agriculture and Life Sciences at UW–Madison.

Simulations in this work were developed using the computing resources and assistance of the Center for High Throughput Computing (2006) in the UW–Madison Department of Computer Sciences. The CHTC is supported by UW–Madison, the Advanced Computing Initiative, the Wisconsin Alumni Research Foundation, the Wisconsin Institutes for Discovery, and the National Science Foundation. This work also employed services of the Open Science Pool as provided by the Open Science Consortium (OSG, 2006; Pordes et al., 2007; Sfiligoi et al.,

2009), which is supported by the National Science Foundation.

References

Ainslie, B., Jackson, P.L., 2011. Investigation into mountain pine beetle above-canopy dispersion using weather radar and an atmospheric dispersion model. Aerobiologia 27, 51–65. https://doi.org/10.1007/s10453-010-9176-9.

Bachmann, K., Keil, C., Craig, G.C., Weissmann, M., Welzbacher, C.A., 2019. Predictability of deep convection in idealized and operational forecasts: effects of radar data assimilation, orography, and synoptic weather regime. Mon. Wea. Rev. 148, 63–81. https://doi.org/10.1175/MWR-D-19-0045.1.

Bauer, S., Shamoun-Baranes, J., Nilsson, C., Farnsworth, A., Kelly, J.F., Reynolds, D.R., Dokter, A.M., Krauel, J.F., Petterson, L.B., Horton, K.G., Chapman, J.W., 2019. The grand challenges of migration ecology that radar aeroecology can help answer. Ecography 42, 861–875. https://doi.org/10.1111/ecog.04083.

Becciu, P., Menz, M.H.M., Aurbach, A., Cabrera-Cruz, S.A., Wainwright, C.E., Scacco, M., Ciach, M., Pettersson, L.B., Maggini, I., Arroyo, G.M., Buler, J.J., Reynolds, D.R., Sapir, N., 2019. Environmental effects on flying migrants revealed by radar. Ecography 42, 942–955. https://doi.org/10.1111/ecog.03995.

Beerwinkle, K.R., Lopez, J.D., Witz, J.A., Schleider, P.G., Eyster, R.S., Lingren, P.D., 1994. Seasonal radar and meteorological observations associated with nocturnal insect flight at altitudes to 900 m. Env. Entomol. 23, 676–683. https://doi.org/10.1093/ee/23.3.676.

Bouchard, M., Auger, I., 2014. Influence of environmental factors and spatio-temporal covariates during the initial development of a spruce budworm outbreak. Landsc. Ecol. 29, 111–126. https://doi.org/10.1007/s10980-013-9966-x.

Bouchard, M., Régnière, J., Therrien, P., 2018. Bottom-up factors contribute to large-scale synchrony in spruce budworm populations. Can. J. For. Res. 48, 277–284. https://doi.org/10.1139/cjfr-2017-0051.

Boulanger, Y., Arseneault, D., 2004. Spruce budworm outbreaks in eastern Quebec over the last 450 years. Can. J. For. Res. 34, 1035–1043. https://doi.org/10.1139/x03-269.

Boulanger, Y., Arseneault, D., Morin, H., Jardon, Y., Bertrand, P., Dagneau, C., 2012. Dendrochronological reconstruction of spruce budworm (Choristoneura fumiferana) outbreaks in southern Quebec for the last 400 years. Can. J. For. Res. 42, 1264–1276. https://doi.org/10.1139/x2012-069.

Boulanger, Y., Fabry, F., Kilambi, A., Pureswaran, D.S., Sturtevant, B.R., Saint-Amant, R., 2017. The use of weather surveillance radar and high-resolution three dimensional weather data to monitor a spruce budworm mass exodus flight. Ag. For. Meteorol. 234–235, 127–135. https://doi.org/10.1016/j.agrformet.2016.12.018.

Browning, K.A., J.C. Nicol, J.H. Marsham, P. Rogberg, and E.G. Norton, 2011: Layers of insect echoes near a thunderstorm and implications for the interpretation of radar data in terms of airflow. Quart. J. Roy. Meteorol. Soc., 137, 723–735, https://doi.org/10.1002/qj.800.

Center for High Throughput Computing, 2006. University of Wisconsin–Madison, Madison, Wisconsin. https://doi.org/10.21231/GNT1-HW21.

Chandra, A.S., Kollias, P., Giangrande, S.E., Klein, S.A., 2010. Long-term observations of the convective boundary layer using insect radar returns at the SGP ARM climate research facility. J. Clim. 23, 5699–5714. https://doi.org/10.1175/2010JCLI3395.1.

Chapman, J.W., Drake, V.A., Reynolds, D.R., 2011. Recent insights from radar studies of insect flight. Ann. Rev. Entomol. 56, 337–356. https://doi.org/10.1146/annurev-ento-120709-144820.

Chapman, J.W., Reynolds, D.R., Wilson, K., 2015. Long-range seasonal migration in insects: mechanisms, evolutionary drivers and ecological consequences. Ecol. Lett. 18, 287–302. https://doi.org/10.1111/ele.12407.

Chapman, J.W., Smith, A.D., Woiwod, I.P., Reynolds, D.R., Riley, J.R., 2002. Development of vertical-looking radar technology for monitoring insect migration. Comp. Electron. Ag. 35, 95–110. https://doi.org/10.1016/S0168-1699(02)00013-3.

Contarini, M., Onufrieva, K.S., Thorpe, K.W., Raffa, K.F., Tobin, P.C., 2009. Mate-finding failure as an important cause of Allee effects along the leading edge of an invading insect population. Entomol. Exp. Appl. 133, 307–314. https://doi.org/10.1111/j.1570-7458.2009.00930.x.

Dargent, F., Candau, J.-N., Studens, K., Perrault, K.H., Reich, M.S., Bataille, C.P., 2023. Characterizing eastern spruce budworm's large-scale dispersal events through flight behavior and stable isotope analyses. Front. Ecol. Evol. 11 https://doi.org/10.3389/fevo.2023.1060982.

Dickison, R.B.B., 1990. Detection of mesoscale synoptic features associated with dispersal of spruce budworm moths in eastern Canada. Phil. Trans. Roy. Soc. London B – Biol. Sci. 328, 607–617. https://doi.org/10.1098/rstb.1990.0131.

Dickison, R.B.B., Haggis, M.J., Rainey, R.C., 1983. Spruce budworm moth flight and storms: case study of a cold front system. J. Clim. Appl. Meteorol. 22, 278–286. doi:10.1175/1520-0450(1983)022<0278:SBMFAS>2.0.CO;2.

Dickison, R.B.B., Haggis, M.J., Rainey, R.C., Burns, L.M.D., 1986. Spruce budworm moth flight and storms: further studies using aircraft and radar. J. Clim. Appl. Meteorol. 25, 1600–1608.doi:10.1175/1520-0450(1986)025<1600:SBMFAS>2.0.CO;2.

Drake, V.A., 1984. The vertical distribution of macro-insects migrating in the nocturnal boundary layer: a radar study. Boundary-Layer Meteorol. 28, 353–374. https://doi.org/10.1007/BF00121314.

Drake, V.A., 1985. Radar observations of moths migrating in a nocturnal low-level jet. Ecol. Entomol. 10, 259–265. https://doi.org/10.1111/j.1365-2311.1985.tb00722.x.

Drake, V.A., Farrow, R.A., 1983. The nocturnal migration of the Australian plague locust, Chortoicetes terminifera (Walker) (Orthoptera: acrididae): quantitative radar observations of a series of northward flights. Bull. Entomol. Res. 73, 567–585. https://doi.org/10.1017/S0007485300009172.

Drake, V.A., Helm, K.F., Readshaw, J.L., Reid, D.G., 1981. Insect migration across Bass Strait during spring: a radar study. Bull. Entomol. Res. 71, 449–466. https://doi.org/10.1017/S0007485300008476.

Draxler, R.R., Hess, G.D., 1998. An overview of the HYSPLIT_4 modeling system for trajectories, dispersion and deposition. Austral. Meteorol. Mag. 47, 295–308.

Gagnon, F., Ibarzabal, J., Savard, J.-P.L., Bélisle, M., Vaillancourt, P., 2011. Autumnal patterns of nocturnal passerine migration in the St. Lawrence estuary region, Quebec, Canada: a weather radar study. Can. J. Zool. 89, 31–46. https://doi.org/10.1139/Z10-092.

Gandiaga, F., James, P.M.A., 2023. Quantifying long-distance dispersal of an outbreaking insect species using trap capture data and phenology. For. Ecol. Manage. 544, 121187 https://doi.org/10.1016/j.foreco.2023.121187.

Garcia, M., Sturtevant, B.R., Saint-Amant, R., Charney, J.J., Delisle, J., Boulanger, Y., Townsend, P.A., Régnière, J., 2022. Modeling weather-driven long-distance dispersal of spruce budworm moths (Choristoneura fumiferana). Part 1: model description. Ag. For. Meteorol. 315, 108815 https://doi.org/10.1016/j.agrformet.2022.108815.

Gauthreaux, S., Diehl, R., 2020. Discrimination of biological scatterers in polarimetric weather radar data: opportunities and challenges. Rem. Sens. 12, 545. https://doi.org/10.3390/rs12030545.

Geerts, B., Damiani, R., Haimov, S., 2006. Finescale vertical structure of a cold front as revealed by an airborne doppler radar. Mon. Wea. Rev. 134, 251–271. https://doi.org/10.1175/MWR3056.1.

Geerts, B., Miao, Q., 2005. Airborne radar observations of the flight behavior of small insects in the atmospheric convective boundary layer. Environ. Entomol. 34, 361–377. https://doi.org/10.1603/0046-225X-34.2.361.

Greenbank, D.O., Schaefer, G.W., Rainey, R.C., 1980. Spruce budworm (Lepidoptera: tortricidae) moth flight and dispersal: new understanding from canopy observations, radar, and aircraft. Mem. Entomol. Soc. Can. 112, 1–49. https://doi.org/10.4039/entm112110fv.

Grimm, V., Berger, U., Bastiansen, F., Eliassen, S., Ginot, V., Giske, J., Goss-Custard, J., Grand, T., Heinz, S.K., Huse, G., Huth, A., 2006. A standard protocol for describing individual-based and agent-based models. Ecol. Modell. 198, 115–126. https://doi.org/10.1016/j.ecolmodel.2006.04.023.

Grimm, V., Berger, U., DeAngelis, D.L., Polhill, J.G., Giske, J., Railsback, S.F., 2010. The ODD protocol: a review and first update. Ecol. Modell. 221, 2760–2768. https://doi.org/10.1016/j.ecolmodel.2010.08.019.

Hu, C., Kong, S., Wang, R., Zhang, F., 2019. Radar measurements of morphological parameters and species identification analysis of migratory insects. Rem. Sens. 11, 1977. https://doi.org/10.3390/rs11171977.

Hu, G., Lim, K.S., Horvitz, N., Clark, S.J., Reynolds, D.R., Sapir, N., Chapman, J.W., 2016. Mass seasonal bioflows of high-flying insect migrants. Science 354, 1584–1587. https://doi.org/10.1126/science.aah4379.

Koralewski, T.E., Wang, H.-H., Grant, W.E., Brewer, M.J., Elliott, N.C., Westbrook, J.K., 2021. Modeling the dispersal of wind-borne pests: sensitivity of infestation forecasts to uncertainty in parameterization of long-distance airborne dispersal. Ag. For. Meteorol. 301-302, 108357 https://doi.org/10.1016/j.agrformet.2021.108357.

Korkmaz, R., Rajabi, H., Eshghi, S., Gorb, S.N., Büscher, T.H., 2023. The frequency of wing damage in a migrating butterfly. Insect Sci. 30, 1507–1517. https://doi.org/10.1111/1744-7917.13153.

Landry, J.-S., Parrott, L., 2016. Could the lateral transfer of nutrients by outbreaking insects lead to consequential landscape-scale effects? Ecosphere 7, e01265. https://doi.org/10.1002/ecs2.1265.

Larroque, J., Legault, S., Johns, R., Lumley, L., Cusson, M., Renaut, S., Levesque, R.C., James, P.M.A., 2019. Temporal variation in spatial genetic structure during population outbreaks: distinguishing among different potential drivers of spatial synchrony. Evol. Appl. 12, 1931–1945. https://doi.org/10.1111/eva.12852.

Lemone, M.A., Zhou, M., Moeng, C.-H., Lenschow, D.H., Miller, L.J., Grossman, R.L., 1999. An observational study of wind profiles in the baroclinic convective mixed layer. Bound. Lay. Meteorol. 90, 47–82. https://doi.org/10.1023/A:1001703303697.

Leskinen, M., Markkula, I., Koistinen, J., Pylkkö, P., Ooperi, S., Siljamo, P., Ojanen, H., Raiskio, S., Tiilikkala, K., 2011. Pest insect immigration warning by an atmospheric dispersion model, weather radars and traps. J. Appl. Entomol. 135, 55–67. https://doi.org/10.1111/j.1439-0418.2009.01480.x.

Liu, D., Zhao, S., Yang, X., Wang, R., Cang, X., Zhang, H., Hu, C., Wyckhuys, K.A.G., Wu, K., 2021. Radar monitoring unveils migration dynamics of the yellow-spined bamboo locust (Orthoptera: arcypteridae). Comp. Electron. Agricul. 187, 106306 https://doi.org/10.1016/j.compag.2021.106306.

Lothon, M., Campistron, B., Chong, M., Couvreux, F., Guichard, F., Rio, C., Williams, E., 2011. Life cycle of a mesoscale circular gust front observed by a C-band Doppler radar in West Africa. Mon. Wea. Rev. 139, 1370–1388. https://doi.org/10.1175/2010MWR3480.1.

Luo, Y., Berbery, E.H., Mitchell, K.E., Betts, A.K., 2007. Relationships between land surface and near-surface atmospheric variables in the NCEP North American regional reanalysis. J. Hydrometeor. 8, 1184–1203. https://doi.org/10.1175/2007JHM844.1.

MacLean, D.A., MacKinnon, W.E., 1996. Accuracy of aerial sketch-mapping estimates of spruce budworm defoliation in New Brunswick. Can. J. For. Res. 26, 2099–2108. https://doi.org/10.1139/x26-238.

McManus, M.L., 1988. Weather, behaviour and insect dispersal. Mem. Entomol. Soc. Can. 120, 71–94. https://doi.org/10.4039/entm120146071-1.

Melnikov, V., Leskinen, M., Koistinen, J., 2014. Doppler velocities at orthogonal polarizations in radar echoes from insects and birds. IEEE Geosci. Rem. Sens. Lett. 11, 592–596. https://doi.org/10.1109/LGRS.2013.2272011.

Mesinger, F., DiMego, G., Kalnay, E., Mitchell, K., Shafran, P.C., Ebisuzaki, W., Jović, D., Woollen, J., Rogers, E., Berbery, E.H., Ek, M.B., Fan, Y., Grumbine, R., Higgins, W., Li, H., Lin, Y., Manikin, G., Parrish, D., Shi, W., 2006. North American regional reanalysis. Bull. Amer. Meteor. Soc. 87, 343–360. https://doi.org/10.1175/BAMS-87-3-343.

Nityananda, V., 2016. Attention-like processes in insects. Proc. Roy. Soc. B: Biol. Sci. 283, 20161986 https://doi.org/10.1098/rspb.2016.1986.

OSG, 2006. Open Science Pool. https://doi.org/10.21231/906P-4D78.

Pedgley, D.E., Reynolds, D.R., Riley, J.R., Tucker, M.R., 1982. Flying insects reveal small-scale wind systems. Weather 37, 295–306. https://doi.org/10.1002/j.1477-8696.1982.tb03518.x.

Pedgley, D.E., Scorer, R.S., Purdom, J.F.W., Simpson, J.E., Wickham, P.G., Dickison, R.B. B., Morris, R.M., Drake, V.A., 1990. Concentration of flying insects by the wind. Phil. Trans. Roy. Soc. London B – Biol. Sci. 328, 631–653. https://doi.org/10.1098/rstb.1990.0133.

Peltonen, M., Liebhold, A.M., Bjørnstad, O.N., Williams, D.W., 2002. Spatial synchrony in forest insect outbreaks: roles of regional stochasticity and dispersal. Ecology 83, 3120–3129.doi:10.1890/0012-9658(2002)083[3120:SSIFIO]2.0.CO;2.

Pordes, R., Petravick, D., Kramer, B., Olson, D., Livny, M., Roy, A., Avery, P., Blackburn, K., Wenaus, T., Würthwein, F., Foster, I., Gardner, R., Wilde, M., Blatecky, A., McGee, J., Quick, R., 2007. The open science grid. J. Phys. Conf. Ser. 78, 012057 https://doi.org/10.1088/1742-6596/78/1/012057.

Powers, J.G., 2017. The Weather Research and Forecasting model: overview, system efforts, and future directions. Bull. Am. Meteorol. Soc. 98, 1717–1737. https://doi.org/10.1175/BAMS-D-15-00308.1.

Rahimzadeh-Bajgiran, P., Weiskittel, A.R., Kneeshaw, D., MacLean, D.A., 2018. Detection of annual spruce budworm defoliation and severity classification using Landsat imagery. Forests 9, 357. https://doi.org/10.3390/f9060357.

Rajabi, H., Dirks, J.-H., Gorb, S.N., 2020. Insect wing damage: causes, consequences and compensatory mechanisms. J. Exp. Biol. 223, jeb215194 https://doi.org/10.1242/jeb.215194.

Régnière, J., 1996. Generalized approach to landscape-wide seasonal forecasting with temperature-driven simulation models. Env. Entomol. 25, 869–881. https://doi.org/10.1093/ee/25.5.869.

Régnière, J., Bolstad, P., 1994. Statistical simulation of daily air temperature patterns in eastern North America to forecast seasonal events in insect pest management. Env. Entomol. 23, 1368–1380. https://doi.org/10.1093/ee/23.6.1368.

Régnière, J., Delisle, J., Pureswaran, D.S., Trudel, R., 2013. Mate-finding allee effect in spruce budworm population dynamics. Entomol. Exp. Appl. 146, 112–122. https://doi.org/10.1111/eea.12019.

Régnière, J., Delisle, J., Sturtevant, B.R., Garcia, M., Saint-Amant, R., 2019a. Modeling migratory flight in the spruce budworm: temperature constraints. Forests 10, 802. https://doi.org/10.3390/f10090802.

Régnière, J., Garcia, M., Saint-Amant, R., 2019b. Modeling migratory flight in the spruce budworm: circadian rhythm. Forests 10, 877. https://doi.org/10.3390/f10100877.

Régnière, J., Lavigne, D., Dickison, R., Staples, A., 1995. Performance Analysis of BioSIM, a Seasonal Pest Management Planning tool, in New Brunswick in 1992 and 1993. Natural Resources Canada, Canadian Forest Service, Laurentian Forestry Centre, Sainte-Foy. QC. Information Report LAU-X-115.

Régnière, J., St-Amant, R., 2007. Stochastic simulation of daily air temperature and precipitation from monthly normals in North America north of Mexico. Int. J. Biometeorol. 51, 415–430. https://doi.org/10.1007/s00484-006-0078-z.

Régnière, J., Saint-Amant, R., Duval, P., 2012. Predicting insect distributions under climate change based on physiological responses: spruce budworm as an example. Biol. Invasions 14, 1–16. https://doi.org/10.1007/s10530-010-9918-1.

Régnière, J., St-Amant, R., Béchard, A., 2014. BioSIM 10 user's manual. Natural Resources Canada, Canadian Forest Service. Laurentian Forestry Centre. Information Report LAU-X-137E. https://cfs.nrcan.gc.ca/publications/download-pdf/34818.

Rennie, S.J., 2014. Common orientation and layering of migrating insects in southeastern Australia observed with a Doppler weather radar. Meteorol. Appl. 21, 218–229. https://doi.org/10.1002/met.1378.

Rennie, S.J., Illingworth, A.J., Dance, S.L., Ballard, S.P., 2010. The accuracy of Doppler radar wind retrievals using insects as targets. Meteorol. Appl. 17, 419–432. https://doi.org/10.1002/met.174.

Reynolds, A.M., Reynolds, D.R., Riley, J.R., 2009. Does a "turbophoretic" effect account for layer concentrations of insects migrating in the stable night-time atmosphere? J. Roy. Soc. Interf. 6, 87–95. https://doi.org/10.1098/rsif.2008.0173.

Reynolds, D.R., Chapman, J.W., Edwards, A.S., Smith, A.D., Wood, C.R., Barlow, J.F., Woiwod, I.P., 2005. Radar studies of the vertical distribution of insects migrating over southern Britain: the influence of temperature inversions on nocturnal layer concentrations. Bull. Entomol. Res. 95, 259–274. https://doi.org/10.1079/BER2005358.

Reynolds, D.R., Riley, J.R., 1988. A migration of grasshoppers, particularly Diabolocatantops axillaris (Thunberg) (Orthoptera: acrididae), in the West African Sahel. Bull. Entomol. Res. 78, 251–271. https://doi.org/10.1017/S000748530001302X.

Reynolds, D.R., Smith, A.D., Chapman, J.W., 2008. A radar study of emigratory flight and layer formation by insects at dawn over southern Britain. Bull. Entomol. Res. 98, 35–52. https://doi.org/10.1017/S0007485307005470.

Rhainds, M., 2010. Female mating failures in insects. Entomol. Exp. Appl. 136, 211–226. https://doi.org/10.1111/j.1570-7458.2010.01032.x.

Rhainds, M., 2015. Wing wear and body size measurements of adult spruce budworms captured at light traps: inference on seasonal patterns related to reproduction. Appl. Entomol. Zool. 50, 477–485. https://doi.org/10.1007/s13355-015-0355-6.

Rhainds, M., 2020. Variation in wing load of female spruce budworms (Lepidoptera: tortricidae) during the course of an outbreak: evidence for phenotypic response to habitat deterioration in collapsing populations. Env. Entomol. 49, 238–245. https://doi.org/10.1093/ee/nvz144.

Rhainds, M., Brodersen, G., 2012. Wing wear of adult Choristoneura fumiferana (Lepidoptera: tortricidae) in relation to age, sex, sex ratio, and presence of host plant. Appl. Entomol. Zool. 47, 475–478. https://doi.org/10.1007/s13355-012-0137-3.

Rhainds, M., Kettela, E.G., 2014. Monitoring spruce budworm with light traps: the effect of trap position. Psyche (Stuttg), 450785. https://doi.org/10.1155/2014/450785.

Rhainds, M., Lavigne, D., Boulanger, Y., DeMerchant, I., Delisle, J., Motty, J., Rideout, T., Labrecque, A., 2022. I know it when I see it: incidence, timing and intensity of immigration in spruce budworm. Ag. For. Entomol. 24, 152–166. https://doi.org/10.1111/afe.12479.

Rhainds, M., Lavigne, D., Rideout, T., Candau, J.-N., 2019. Temporal variation in abundance of male and female spruce budworms at combinatory associations of light traps and pheromone traps. Entomol. Exp. Appl. 167, 526–533. https://doi.org/10.1111/eea.12806.

Riley, J.R., Reynolds, D.R., 1983. A long-range migration of grasshoppers observed in the Sahelian zone of Mali by two radars. J. Animal Ecol. 52, 167–183. https://doi.org/10.2307/4594.

Riley, J.R., Reynolds, D.R., Charles, R.R., 1979. Radar-based studies of the migratory flight of grasshoppers in the middle Niger area of Mali. Proc. Roy. Soc. London B – Biol. Sci. 204, 67–82. https://doi.org/10.1098/rspb.1979.0013.

Riley, J.R., Reynolds, D.R., Smith, A.D., L.J, Rosenberg, Xia-nian, C., Xiao-xi, Z., Guo-min, X., Ji-yi, C., Ai-dong, B., Bao-ping, Z., Hai-kou, W., 1994. Observations on the autumn migration of Nilaparvata lugens (Homoptera: delphacidae) and other pests in east central China. Bull. Entomol. Res. 84, 389–402. https://doi.org/10.1017/S0007485300032521.

Roberts, N.M., Lean, H.W., 2008. Scale-selective verification of rainfall accumulations from high-resolution forecasts of convective events. Mon. Wea. Rev. 136, 78–97. https://doi.org/10.1175/2007MWR2123.1.

Sanders, C.J., 1983. Local dispersal of male spruce budworm (Lepidoptera tortricidae) moths determined by mark, release, and recapture. Can. Entomol. 115, 1065–1070. https://doi.org/10.4039/Ent1151065-9.

Sanders, C.J., 1987. Flight and copulation of female spruce budworm in pheromone-permeated air. J. Chem. Ecol. 13, 1749–1758. https://doi.org/10.1007/BF00980215.

Satterfield, D.A., Sillett, T.S., Chapman, J.W., Altizer, S., Marra, P.P., 2020. Seasonal insect migrations: massive, influential, and overlooked. Front. Ecol. Environ. 18, 335–344. https://doi.org/10.1002/fee.2217.

Schaefer, G.W., 1969. Radar studies of locust, moth and butterfly migration in the Sahara. Proc. R. Entomol. Soc. Lond. C 34, 33. https://doi.org/10.1111/j.1946-150X.1969.tb00569.x.

Schaefer, G.W., 1976. Radar observations of insect flight. Symp. R. Entomol. Soc. Lond. 7, 157–197.

Schaefer, G.W., 1979. An airborne radar technique for the investigation and control of migrating pest species. Phil. Trans. R. Soc. Lond. B 287, 459–465. https://doi.org/10.1098/rstb.1979.0077.

Sfiligoi, I., Bradley, D.C., Holzman, B., Mhashilkar, P., Padhi, S., Wurthwein, F., 2009. The pilot way to grid resources using glideinWMS. In: Proceedings of the 2009 WRI World Congress on Computer Science and Information Engineering, 2, pp. 428–432. https://doi.org/10.1109/CSIE.2009.950.

Skamarock, W.C., Klemp, J.B., 2008. A time-split nonhydrostatic atmospheric model for weather research and forecasting applications. J. Comp. Phys. 227, 3465–3485. https://doi.org/10.1016/j.jcp.2007.01.037.

Skamarock, W.C., J.B. Klemp, J. Dudhia, D.O. Gill, D.M. Barker, M.G. Duda, X.-Y. Huang, W. Wang, and J.G. Powers, 2008: A description of the Advanced Research WRF version 3. NCAR Tech. Note NCAR/TN-475+STR, 113 pp., https://doi.org/10.5065/D68S4MVH.

Stein, A.F., Draxler, R.R., Rolph, G.D., Stunder, B.J.B., Cohen, M.D., Ngan, F., 2015. NOAA's HYSPLIT atmospheric transport and dispersion modeling system. Bull. Amer. Meteorol. Soc. 96, 2059–2077. https://doi.org/10.1175/BAMS-D-14-00110.1.

Stepanian, P.M., Horton, K.G., Melnikov, V.M., Zrnić, D.S., Gauthreaux, S.A., 2016. Dual-polarization radar products for biological applications. Ecosphere 7, e01539. https://doi.org/10.1002/ecs2.1539.

Stull, R.B., 1988. An Introduction to Boundary Layer Meteorology. Kluwer Academic Publishers, p. 670. ISBN 9027727694.

Sturtevant, B.R., Achtemeier, G.L., Charney, J.J., Anderson, D.P., Cooke, B.J., Townsend, P.A., 2013. Long-distance dispersal of spruce budworm (Choristoneura fumiferana Clemens) in Minnesota (USA) and Ontario (Canada) via the atmospheric pathway. Ag. For. Meteorol. 168, 186–200. https://doi.org/10.1016/j.agrformet.2012.09.008.

Sun, J., Lenschow, D.H., Burns, S.P., Banta, R.M., Newsom, R.K., Coulter, R., Frasier, S., Ince, T., Nappo, C., Balsley, B.B., Jensen, M., Mahrt, L., Miller, D., Skelly, B., 2004. Atmospheric disturbances that generate intermittent turbulence in nocturnal boundary layers. Bound.-Lay. Meteorol. 110, 255–279. https://doi.org/10.1023/A:1026097926169.

Taylor, S.L., MacLean, D.A., 2008. Validation of spruce budworm outbreak history developed from aerial sketch mapping of defoliation in New Brunswick. North. J. Appl. For. 25, 139–145. https://doi.org/10.1093/njaf/25.3.139.

Wang, H.-H., Grant, W.E., Elliott, N.C., Brewer, M.J., Koralewski, T.E., Westbrook, J.K., Alves, T.M., Sword, G.A., 2019. Integrated modelling of the life cycle and aeroecology of wind-borne pests in temporally-variable spatially-heterogeneous environment. Ecol. Model. 399, 23–38. https://doi.org/10.1016/j.ecolmodel.2019.02.014.

Westbrook, J.K., Eyster, R.S., 2017. Doppler weather radar detects emigratory flights of noctuids during a major pest outbreak. Rem. Sens. Appl.: Soc. Env. 8, 64–70. https://doi.org/10.1016/j.rsase.2017.07.009.

Westbrook, J.K., Eyster, R.S., Wolf, W.W., 2014. WSR-88D doppler radar detection of corn earworm moth migration. Int. J. Biometeorol. 58, 931–940. https://doi.org/10.1007/s00484-013-0676-5.

Westbrook, J., Fleischer, S., Jairam, S., Meagher, R., Nagoshi, R., 2019. Multigenerational migration of fall armyworm, a pest insect. Ecosphere 10, e02919. https://doi.org/10.1002/ecs2.2919.

Westbrook, J.K., Isard, S.A., 1999. Atmospheric scales of biotic dispersal. Ag. For. Meteorol. 97, 263–274. https://doi.org/10.1016/S0168-1923(99)00071-4.

Westbrook, J.K., Nagoshi, R.N., Meagher, R.L., Fleischer, S.J., Jairam, S., 2016. Modeling seasonal migration of fall armyworm moths. Int. J. Biometeorol. 60, 255–267. https://doi.org/10.1007/s00484-015-1022-x.

Williams, D.W., Liebhold, A.M., 2000. Spatial synchrony of spruce budworm outbreaks in eastern North America. Ecology 81, 2753–2766. https://doi.org/10.1890/0012-9658(2000)081[2753:SSOSBO]2.0.CO;2.

Willmott, A.P., Ellington, C.P., 1997a. The mechanics of flight in the hawkmoth Manduca sexta. I. Kinematics of hovering and forward flight. J. Exp. Biol. 200, 2705–2722. https://doi.org/10.1242/jeb.200.21.2705.

Willmott, A.P., Ellington, C.P., 1997b. The mechanics of flight in the hawkmoth Manduca sexta. II. Aerodynamic consequences of kinematic and morphological variation. J. Exp. Biol. 200, 2723–2745. https://doi.org/10.1242/jeb.200.21.2723.

Wood, C.R., Chapman, J.W., Reynolds, D.R., Barlow, J.F., Smith, A.D., Woiwod, I.P., 2006. The influence of the atmospheric boundary layer on nocturnal layers of noctuids and other moths migrating over southern Britain. Int. J. Biometeorol. 50, 193. https://doi.org/10.1007/s00484-005-0014-7.

Wood, C.R., Reynolds, D.R., Wells, P.M., Barlow, J.F., Woiwod, I.P., Chapman, J.W., 2009. Flight periodicity and the vertical distribution of high-altitude moth migration over southern Britain. Bull. Entomol. Res. 99, 525–535. https://doi.org/10.1017/S0007485308006548.

Wood, C.R., Clark, S.J., Barlow, J.F., Chapman, J.W., 2010. Layers of nocturnal insect migrants at high-altitude: the influence of atmospheric conditions on their formation. Ag. For. Entomol. 12, 113–121. https://doi.org/10.1111/j.1461-9563.2009.00459.x.

Zrnic, D.S., Ryzhkov, A.V., 1998. Observations of insects and birds with a polarimetric radar. IEEE Trans. Geosci. Rem. Sens. 36, 661–668. https://doi.org/10.1109/36.662746.